

Copyright
by
Luis Octavio Yepez Roca
1997

**ACOUSTIC EMISSION EXAMINATION OF HIGH
STRENGTH PRESTRESSED CONCRETE GIRDERS**

by

Luis Octavio Yopez Roca, B.S.C.E.

Thesis

Presented to the Faculty of the Graduate School of

The University of Texas at Austin

in Partial Fulfillment

of the Requirements

for the Degree of

Master of Science in Engineering

The University of Texas at Austin

August 1997

**ACOUSTIC EMISSION EXAMINATION OF HIGH
STRENGTH PRESTRESSED CONCRETE GIRDERS**

**Approved by
Supervising Committee:**

Timothy J. Fowler

Ned H. Burns

Howard M. Liljestrang

to my wife, María Fernanda, who supported me with unconditional love and care

Acknowledgements

I would like to express my gratitude to all the people who contributed to this project, from beginning to end. Without them, all of this work would not have been possible.

Fundacyt-Ecuador, funding my scholarship, gave me the opportunity to look for a research project of my interest. My thanks to all the staff and Board of Directors.

Kim Killingsworth at Laspau deserves recognition. She was always working on my behalf.

My wife helped me put together half of the tests. Without her help, I would not have complete my testing program on time.

I would like to express my deepest gratitude to my advisor, Dr. Tim Fowler, who gave me all the support necessary to undertake a project like this. He was always ready to help in whatever was required, and with his friendly advise and good humor, kept me motivated. He will always be an inspiration to me, in my professional career.

My sincere thanks to Chuck Barnes. He started the difficult process of teaching me the AE technique. He shared his experience with me. His guidance and comments are greatly appreciated.

The “AE team” deserves recognition for their support. Yajai Promboon, Parry Berkowitz, and Paul Ziehl shared the AE lab in a friendly manner.

Robbie Barnes played a crucial role in my work. He and his co-workers were extremely patient during the tests, bearing with all the waiting and problems derived. It was a pleasure for me to work with such a nice group of people.

My thanks to the staff at Ferguson Lab. Their cooperation was very valuable, from start to end. Everyone was very diligent, and prompt to help me.

I am very grateful to Physical Acoustics Corporation. Mark Carlos and John Romaine solved my problems on request. They played a vital part in the completion of this thesis, accepting suggestions about the software and making them available immediately.

My thanks to the Texas Department of Transportation (TxDOT). I had the splendid opportunity to do the research on the Research Project 0-1388.

Finally, I would like to express my gratitude to Dr. Ned Burns. He did not hesitate to support my research program at any time. His disposition and comments to the work done are greatly appreciated.

August, 1997

ACOUSTIC EMISSION EXAMINATION OF HIGH STRENGTH PRESTRESSED CONCRETE GIRDERS

Luis Octavio Yopez Roca, M.S.E.

The University of Texas at Austin, 1997

Supervisor: Timothy J. Fowler

High strength prestressed concrete girders were monitored with acoustic emission equipment, during load tests, to determine the possibility of crack prediction and location prior to their appearance at the surface. Three basic events and zones were monitored: shear-induced cracking in the web, flexural cracking at the region of maximum moment, and strand slippage at the anchorage zone. The research was directed to basic parametric analysis, source location, moment tensor analysis using a 6 channel digital AE instrument, and development of criteria for AE use on concrete bridge girders. The test results show a significant increase in cumulative energy shortly before shear and flexural cracking was observed on the surface. A good agreement between located and classified sources with actual crack pattern was observed.

Table of Contents

List of Tables.....	xi
List of Figures	xii
List of Illustrations	xvi
CHAPTER 1	
INTRODUCTION.....	1
1.1 introduction	1
1.2 Acoustic Emission.....	2
1.2.1 The Acoustic Emission Signal	3
1.2.2 Instrumentation.....	5
1.2.3 Characteristics of the Method	7
CHAPTER 2	
LITERATURE REVIEW	9
2.1 Introduction	9
2.2 Problems of Acoustic Emission in Concrete.....	10
2.2.1 Material Heterogeneity.....	10
2.2.2 Microcracking and Wave Attenuation	11
2.2.3 Surface Condition.....	12
2.3 Materials and Mechanisms Studied.....	13
2.4 Tools for Acoustic Emission Analysis	16
2.4.1 Instrumentation.....	16
2.4.2 Parameters	17
2.4.3 Analytical Advances	19

CHAPTER 3

EXPERIMENTAL PROGRAM.....	23
3.1 Introduction	23
3.2 Objectives of the Testing Program.....	24
3.3 Test Sample	24
3.4 Test Setup	26
3.4.1 Beam Setup	26
3.4.2 Instrumentation.....	27
SENSORS	27
ACOUSTIC EMISSION SYSTEMS	31
3.5 Testing Procedure.....	32
3.5.1 Calibration.....	32
3.5.2 Data Acquisition.....	32

CHAPTER 4

ANALYSIS OF RESULTS.....	34
4.1 Introduction	34
4.2 Group I - Parametric Tests	35
4.2.1 Test M0B0S.....	35
4.2.2 Test M0B0N	41
4.2.3 Test M0B1N.....	45
4.2.4 Test M0B1S.....	48
4.2.5 Test H0B0N.....	52
4.2.6 Test H0B0S	56
4.2.7 Test H0B1S	61
4.2.8 Test H0B1N.....	65
4.3 Summary of Parametric Tests	69
4.4 Group II Tests - Source Location and Moment Tensor Analysis	72

4.4.1 Test L4B0S.....	72
4.4.2 Test L4B1N.....	77

CHAPTER 5

CONCLUSIONS AND RECOMMENDATIONS.....	88
5.1 Conclusions.....	88
5.2 Recommendations.....	90
REFERENCES.....	93
VITA.....	97

List of Tables

Table 3.1 Characteristics of the test beams.....	25
Table 3.2 General overview of the test program.....	31
Table 4.1 Summary of results of parametric tests.....	69
Table 4.2 Event coordinates and type, Test L4B0S	75
Table 4.3a Event coordinates and type, Test L4B1N (continued on next page as Table 4.3b).	78
Table 4.3b Event coordinates and type, Test L4B1N (continued).	79

List of Figures

Figure 1.1 Acoustic emission signal plotted against time, showing typical parameters.	3
Figure 1.2 Envelope of rectified signal.	4
Figure 1.3 Acoustic emission sensor.....	6
Figure 2.1 Kaiser and Felicity effect in a load/reload test.	18
Figure 3.1 AASHTO Type I girder with slab cast on top.	25
Figure 3.2 Test setup showing frame and specimen.	26
Figure 3.3 Location of sensors for group I, showing cracking zones.	27
Figure 3.4 Typical sensor locations on Group I, seven sensor array.	28
Figure 3.5 Array of sensors for Moment Tensor Analysis in Test L4B0S.	29
Figure 3.6 Array of sensors for Moment Tensor Analysis in Test L4B1N.....	29
Figure 3.7 Detail of sensor mounting device.	30
Figure 4.1 Plot of cumulative signal strength vs. time of Test M0B0S.	35
Figure 4.2a Historic index vs. time plot of Test M0B0S.	36
Figure 4.2b Expanded historic index vs. time plot of Test M0B0S.....	37
Figure 4.3 Log duration vs. amplitude plot of Test M0B0S up to t=1200 sec.....	38
Figure 4.4 Log duration vs. amplitude plot of Test M0B0S up to t=2000 sec.....	39
Figure 4.5 Log duration vs. amplitude plot of Test M0B0S up to t=3200 sec.....	40
Figure 4.6 Cumulative signal strength vs. time plot of Test M0B0N.	41
Figure 4.7a Historic index vs. time plot of Test M0B0N.....	42
Figure 4.7b Expanded historic index vs. time plot of Test M0B0N.	43

Figure 4.8	Log duration vs. amplitude plot of Test M0B0N up to t=1200 sec....	43
Figure 4.9	Log duration vs. amplitude plot of Test M0B0N up to t=2000 sec....	44
Figure 4.10	Log duration vs. amplitude plot of Test M0B0N up to t=3000 sec.	44
Figure 4.11	Cumulative signal strength vs. time plot of Test M0B1N.	45
Figure 4.12	Historic index vs. time plot of Test M0B1N.	46
Figure 4.13	Log duration vs. amplitude plot of Test M0B1N up to t=2000 sec.	47
Figure 4.14	Log duration vs. amplitude plot of Test M0B1N up to t=3200 sec.	47
Figure 4.15	Cumulative signal strength vs. time plot of Test M0B1S.	48
Figure 4.16	Historic index vs. time plot of Test M0B1S.	49
Figure 4.17	Log duration vs. amplitude plot of Test M0B1S up to t=1200 sec...	50
Figure 4.18	Log duration vs. amplitude plot of Test M0B1S, ch.: 14-17, t=1200 sec.	51
Figure 4.19	Log duration vs. amplitude plot of Test M0B1S, ch.: 14-17, t=2000 sec.	51
Figure 4.20	Log duration vs. amplitude plot of Test M0B1S, ch.: 14-17, t=3200 sec.	52
Figure 4.21	Cumulative signal strength vs. time plot of Test H0B0N.	53
Figure 4.22a	Historic index vs. time plot of Test H0B0N.	54
Figure 4.22b	Expanded historic index vs. time plot of Test H0B0N.	54
Figure 4.23	Log duration vs. amplitude plot of Test H0B0N up to t=1000 sec...	55
Figure 4.24	Log duration vs. amplitude plot of Test H0B0N up to t=1800 sec...	55

Figure 4.25	Log duration vs. amplitude plot of Test H0B0N up to t=2600 sec...	56
Figure 4.26	Cumulative signal strength vs. time plot, Test H0B0S, ch.: 13-17. .	57
Figure 4.27	Cumulative signal strength vs. time plot, Test H0B0S, ch.: 19-20. .	57
Figure 4.28	Historic Index vs. time plot of Test H0B0S, ch.: 13-17.	58
Figure 4.29	Historic index vs. time plot of Test H0B0S, ch.: 19-20.....	58
Figure 4.30	Log duration vs. amplitude plot of Test H0B0S up to t=900 sec.	59
Figure 4.31	Log duration vs. amplitude plot of Test H0B0S up to t=2000 sec. ..	60
Figure 4.32	Log duration vs. amplitude plot of Test H0B0S up to t=3200 sec. ..	60
Figure 4.33	Cumulative signal strength vs. time plot, Test H0B1S, ch.: 13-17. .	61
Figure 4.34	Cumulative signal strength vs. time plot, Test H0B1S, ch.: 19-20. .	62
Figure 4.35a	Historic index vs. time plot of Test H0B1S, ch.: 13-17.....	62
Figure 4.35b	Expanded historic index vs. time plot, Test H0B1S, ch.: 13-17.....	63
Figure 4.36	Historic index vs. time plot of Test H0B1S, ch.: 19-20.....	63
Figure 4.37	Log duration vs. amplitude plot of Test H0B1S up to t=800 sec.	64
Figure 4.38	Log duration vs. amplitude plot of Test H0B1S up to t=2000 sec. ..	64
Figure 4.39	Log duration vs. amplitude plot of Test H0B1S up to t=3000 sec. ..	65
Figure 4.40	Cumulative signal strength vs. time plot, Test H0B1N, ch: 13-17...	66
Figure 4.41	Cumulative signal strength vs. time plot, Test H0B1N, ch.: 19- 20.....	66
Figure 4.42	Historic index vs. time plot of Test H0B1N, ch.: 13-17.....	67
Figure 4.43	Log duration vs. amplitude plot of Test H0B1N, t=800 sec, all channels.....	67
Figure 4.44	Log duration vs. amplitude plot of Test H0B1N, t=1800 sec, all channels.....	68

Figure 4.45	Log duration vs. amplitude plot of Test H0B1N, $t=2400$ sec, all channels.....	68
Figure 4.46	Ratio of load at onset of emission to first cracking load and to ultimate load as a function of test sample.	70
Figure 4.47	Cumulative signal strength at onset of AE and at first cracking as a function of test sample.....	71
Figure 4.48	Historic index at onset of AE and at first cracking as a function of test sample.	71
Figure 4.49	Typical waveforms used for source location and moment tensor analysis.	73
Figure 4.50	Location of events and crack pattern of Test L4B0S.....	76
Figure 4.51	Sensor locations of Test L4B1N.....	80
Figure 4.52	Event locations at $P=110$ k, Test L4B1N.	81
Figure 4.53	Event locations at $P=110$ k, Test L4B1N, end view.....	81
Figure 4.54	West face view of the first crack at $P=130$ k, Test L4B1N.	82
Figure 4.55	East face view of the first crack at $P=130$ k, Test L4B1N.	83
Figure 4.56	Event locations and crack pattern at $P=130$ k, Test L4B1N.....	83
Figure 4.57	Event locations at $P=130$ k, Test L4B1N, end view.....	84
Figure 4.58	West face view of cracks at $P=161$ k, Test L4B1N.....	84
Figure 4.59	East face view of cracks at $P=161$ k, Test L4B1N.	85
Figure 4.60	Event locations at $P=135$ k and crack pattern at $P=160$ k, Test L4B1N.....	86
Figure 4.61	Event locations at $P=161$ k, Test L4B1N, end view.....	86

List of Illustrations

Illustration 4.1 Sample output of program Sigma.	74
---	----

CHAPTER 1

INTRODUCTION

1.1 INTRODUCTION

A solid body subjected to stress emits transient elastic waves due to several causes such as moving dislocations, crack growth, sliding grain boundaries and corrosion. This phenomena is known as acoustic emission (AE). It can be measured with proper instrumentation and is used to give an idea of the current structural condition of a structure which is to be evaluated.

Acoustic emission as a non-destructive test method (NDT) was first used by J. Kaiser in 1950 ^[1] and has since become a powerful tool for non-destructive evaluation (NDE) in metal and reinforced plastic structures, and to a lesser extent in concrete applications. The greatest advance in the field has been in the electronics of the instrumentation. The equipment available today is capable of acquiring data at very high rates and can perform real time waveform analysis. In research applications this is used for source location, acoustic emission event characterization, and study of the signals.

Comprehensive analysis of acoustic emission in metals and plastics, enhanced by the continuity and consistency of these two materials, has led to the specification of standards for metal tank car and pressure vessel testing ^[2,6] and

for FRP pressure and atmospheric vessels ^[3]. Concrete applications instead, are still at an experimental stage due mostly to material heterogeneity and high attenuation of the acoustic emission signals. The latter can be explained by the existence of internal microcracking or shrinkage cracks ^[4].

A prestressed concrete element, however, remains uncracked until it reaches a high percentage of its ultimate load. The force exerted by the prestressing strands prevents the growth of initial cracks and results in lower attenuation compared to reinforced concrete.

1.2 ACOUSTIC EMISSION

The ASTM E1316 Standard Terminology for Non-Destructive Examinations defines acoustic emission as:

“The class of phenomena whereby transient elastic waves are generated by the rapid release of energy from localized sources within a material, or the transient waves so generated.”

Acoustic emission signals can be detected by instrumentation mounted on the surface of the element under test. Normally, a parametric study is performed using the signal analysis capabilities of the equipment. This data is used to locate areas where stresses might be growing to an undesirable high level, to assess structural integrity, to correlate theoretical predictions with observed behavior, or to establish evaluation criteria for use of AE as a non-destructive technique (NDT).

1.2.1 The Acoustic Emission Signal

The acoustic emissions generated by any causal event propagate from its source within the body to the sensor, usually located on the surface, in much the same way as earthquake waves travel through the earth. During this travel the signal is attenuated. High frequency components are attenuated more than low frequency components, and sensors located far away from the source receive only the low frequency components of the wave. The range of frequencies observed for acoustic emissions usually falls within 10 kHz to 30 MHz, and depending on the type of sensors used, low-pass, high-pass or band pass filters modify the received signal for the required analysis.

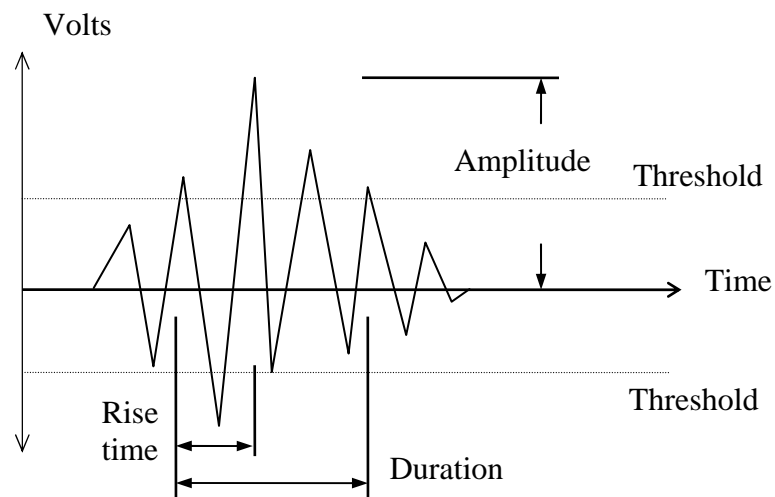


Figure 1.1 Acoustic emission signal plotted against time, showing typical parameters.

Figure 1.1 shows the output from an AE sensor. When the signal rises above the threshold, the sensor is said to have received a hit. Several parameters that can be obtained from a signal, and can be used to characterize events occurring in the material. For example, events with increasing amplitude might be related to the initiation of yielding in steel or cracking of a composite matrix. The parameters such as, duration, rise time, and amplitude are referred to as hit attributes.

There are certain settings that must be specified by the user of the technique such as the threshold value. It is used to selectively reject signals with amplitude below a certain level which will not provide useful information as they may correspond to ambient, electronic, or electromagnetic noise.

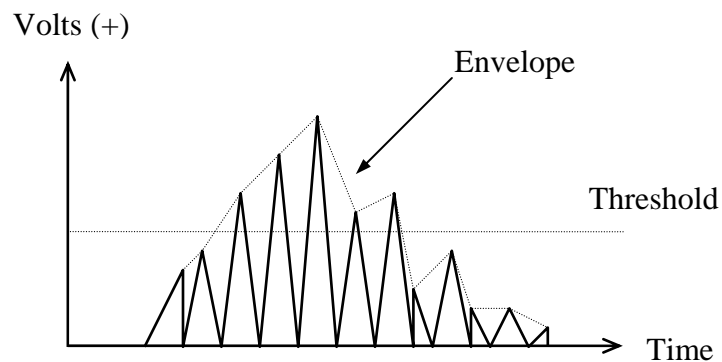


Figure 1.2 Envelope of rectified signal.

Although the real signal input is of the type presented in Fig. 1.1, most instrumentation uses the rectified signal as appears in Fig. 1.2 to perform the required analysis. Another important parameter is the area under the envelope of the signal. This is known as the signal strength or relative energy. Signal strength is a valuable evaluation parameter in that it can reduce the attenuation effects. The signal experiences a loss of high frequency components and a decrease in amplitude during travel, and is transformed to a longer low frequency signal which maintains the same approximate area under the envelope.

Another parameter used mostly in old instrumentation is ringdown counts, or counts, which refers to the number of threshold crossings of the signal. This has been replaced by duration because in odd shaped signals the counts may give an erroneous representation of the duration of the event ^[5]. Counts is also sensitive to the frequency of the sensor. A 100 kHz sensor will record half as many counts as a 200 kHz sensor when recording the same duration hit.

1.2.2 Instrumentation

The instrumentation for acoustic emission testing consists of two main components: the sensors and the measurement circuitry.

The sensors capture the change in pressure on the surface and convert it to an electrical signal by means of a piezoelectric crystal inside a metal housing (see Fig. 1.3). In some sensors, a preamplifier, which is needed to overcome voltage losses between the sensor and the instrumentation, is built into the housing to reduce the inherent noise level. A coupling compound must be used to provide a

good contact between the wear plate of the sensors and the mounting surface, which sometimes, and especially in the case of concrete, is very rough.

The principal types of sensors are : a) resonant at a particular frequency and b) broadband. The resonant sensors are very sensitive at the resonant frequency and may also be constructed with a low and high-pass filter to eliminate the undesired ranges. Broadband sensors, used for frequency spectrum analysis, may be constructed with a flat response range between typical values of 50 kHz and 1 MHz.

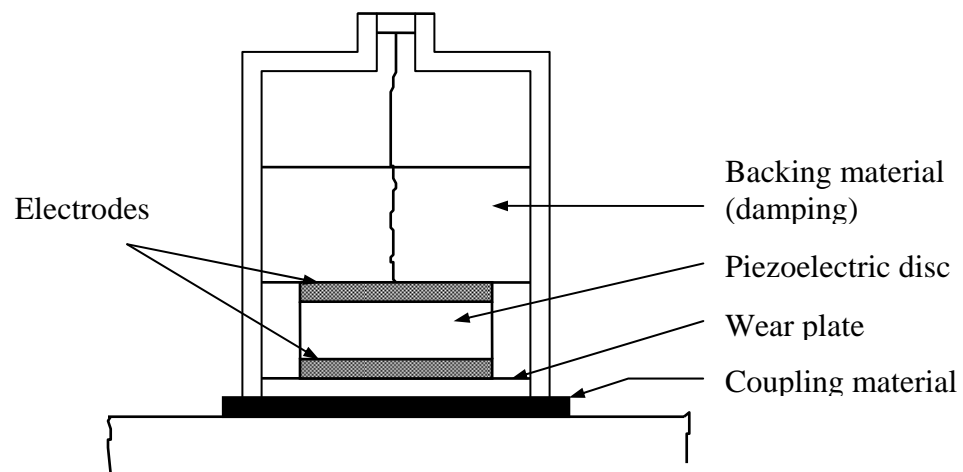


Figure 1.3 Acoustic emission sensor

The sensors used in the same test are calibrated and compared to each other to account for variations in sensitivity. This is accomplished by means of

waves generated by artificial sources. Breakage of a Pentel 0.3 mm 2H pencil lead is known as the Hsu-Nielsen source. Breakage of a 0.2 mm diameter glass capillary tube, an electric spark, helium gas jet and acoustic emission simulators have also been used as alternative techniques ^[1].

The measurement circuitry is more varied, depending on the particular manufacturer. The simple instruments will capture the basic parameters discussed previously with a clock precision of milliseconds (10^{-3} sec) and store them into a disk. The more sophisticated will work with a precision up to 100 nanoseconds (10^{-7} sec) which makes them suitable for source location estimates where the timing of the events becomes critical. Others will digitize and store the signal for post-test waveform analysis, also presenting it in real time on a display screen. This consumes a great amount of data storage space and must be taken into account in planning the test.

1.2.3 Characteristics of the Method

Acoustic emission has many applications in several fields. As mentioned before, these applications are mainly in metals and composites ^[2,3,6]. The method is a global technique, meaning that a large volume of the material, if not all, may be tested at the same time, depending on the stress conditions of the structure. The detection of discontinuities in inaccessible areas is also a well recognized ability, since the waves travel through the body and reach sensors located nearby. Perhaps the most valuable characteristic is its ability to provide a real time indication of growing discontinuities. This is a valuable tool in field structures

such as bridges, where the monitoring can be done in-situ and for any period in order to collect the necessary information to assess the condition of the structure. On-line monitoring is another capability which proves useful in industry where large containment structures can be tested without interrupting the production process by pressurizing the contained materials to obtain the necessary stress state.

Acoustic emission, as with any other non-destructive technique, has its disadvantages. It is very dependent on the loading method, because discontinuities in unstressed areas might not be detected. Also, the geometry of the structure and the attenuation characteristics of the constituent materials might conceal the emissions. Even in well established applications, such as in metal tank car testing, it is not possible to determine the size of a defect. Another drawback is the lack of a standardized procedure for data interpretation.

Despite the difficulties encountered with the method, once the technique has been mastered for a specific application, acoustic emission testing will provide reliable information for the evaluation of the structure and the need for repair.

CHAPTER 2

LITERATURE REVIEW

2.1 INTRODUCTION

The acoustic emission (AE) method is a promising technique for non-destructive testing of big structures due to its global nature. A defective area can be isolated and then investigated locally by other methodology. Concrete materials and structures could benefit from this technique. Unfortunately, AE in concrete, as used today, is still at an experimental stage. Although several field studies with AE have been performed successfully, work being conducted at research laboratories throughout the world deals mostly with small size specimens and highly controlled environments. Direct application to field problems and full scale elements is more complicated. However, interest in the subject is growing due to advances in digital computers and electronic instrumentation and a continuous effort from the research community to discover the relationship between acoustic emission and the wide variety of mechanisms that play a role in concrete composition and behavior.

The difficulties encountered when running an acoustic emission test in concrete are discussed in this chapter, along with the type of cement based materials currently being studied. Different mechanisms investigated and the

tools used for analysis are reviewed. The basic waveform parameters and recently developed data analysis techniques are presented, together with an assessment of the current standing of acoustic emission research in the concrete field.

2.2 PROBLEMS OF ACOUSTIC EMISSION IN CONCRETE

A test performed with acoustic emission in concrete has to overcome a number of obstacles not encountered in other more uniform materials, such as steel and fiber reinforced plastics. This is reflected by the absence of a standard procedure to conduct AE tests of concrete materials, in contrast to the well defined testing procedures and evaluation criteria developed for use with new and in-service metal structures such as pressure vessels, atmospheric storage tanks, railroad tank cars ^[2,6,7], and with pressurized and atmospheric FRP containment structures ^[3,8].

The principal difficulties encountered in concrete testing are discussed in the following sections.

2.2.1 Material Heterogeneity

Concrete is by nature a heterogeneous material, and several factors contribute to this.

Different aggregate sources, cements and additives, and water quality used in a mix, produce large variations in material characteristics. Also, the fact that concrete is produced in many locations by a variety of producers, using several

manufacturing processes, contributes to the range of materials known as “concrete”. This is in contrast to materials like steel, which are manufactured in a highly controlled environment and by a limited number of industries.

Actual ambient test conditions can vary, and this further adds to the uncertainty. The relative humidity of the environment is an important factor to consider. Uomoto et al ^[9] shows that this effect is perhaps more important than the variation in the W/C ratio of the mix. Concrete in environments with different measured degrees of humidity, exhibit different wave velocities and attenuation characteristics.

2.2.2 Microcracking and Wave Attenuation

Wave travel is affected by the inherent microcracking present in concrete ^[4] and by its composite nature. Even at very low stresses, microcracking starts to grow extensively inside the element until it becomes a well developed crack network with surface breaking cracks. This causes high rates of emission even at early stages of loading, requiring considerable amounts of data storage capacity.

The wave characteristics of the signal are largely affected by the size of the discontinuities present. If a 300 kHz resonant sensor is chosen for a test, and assuming a typical wave velocity for concrete as 4000 m/s, the wavelength can be obtained from the following equation:

$$\lambda = c / f$$

where λ is the wavelength, c is the wave velocity and f is the wave frequency. From the previous values a wavelength of 13 mm is obtained. This means that an obstacle of this size will be enough to reflect the traveling waves. Obviously, this is the order of magnitude for concrete aggregate size. Testing on this subject is reported by Uomoto et al ^[9], where attenuation due to distance of the source from the transducer was measured to be of the order of 1 dB per centimeter.

2.2.3 Surface Condition

Mounting the sensors can be a difficult task if voids, dust or loose particles are present on the surface. Actual structures might display this characteristic, particularly due to weathering. Irregularities due to voids or exposed aggregate must be avoided. Voids, which always appear in concrete surfaces, sometimes hinder the placement of sensors in key locations, forcing placement in adjacent areas, which might not be as appropriate.

Good contact between the sensor's wear plate and the concrete surface is necessary in order to get reliable signals, so a coupling material such as a mineral grease is used. Also, attention must be given to the weight of the sensor and the way it is fixed to the element, especially in vertical and underside surfaces, since gravity can easily diminish the contact pressure between the sensor and the concrete surface.

2.3 MATERIALS AND MECHANISMS STUDIED

Among the different cementitious materials, the ones being studied the most are Portland cement mortar and concrete beams. AE parameter and source location experiments in the hardened state indicating fracture were carried out ^[10,11]. AE is used to determine the extent and propagation characteristics of the fracture process zone.

In the fresh state, Portland cement concrete has been monitored with AE to observe the phase transformations during the setting process ^[12]. Similarly, a real-time application to process control in the mixing and placement of roller compacted concrete for dam construction was reported by Ohtsu ^[13]. It was found that the gradient of AE energy to mixing time changes indicated a shift from granular phase to liquid phase of the material inside the mixing drum, helping to optimize mixing time.

Plain concrete studies in beams have been reported by Nielsen et al ^[14]. The loading history of concrete specimens was monitored, using the Kaiser effect as the primary evaluation criteria.

Prestressed concrete elements have been analyzed, although only in field applications ^[15,16]. Acoustic emission was used to monitor the performance of buried prestressed concrete cylinder pipes in service. Also, in-service prestressed bridge girders were monitored to investigate the suitability of the technique for structural monitoring, and a previously repaired crack in a prestressed concrete box girder was found to be acoustically active.

Additions such as silica fume and synthetic fibers have been studied in order to obtain a better understanding of their influence in a concrete mix. Concrete with silica fume additions was monitored with acoustic emission and compared with air permeability tests. The purpose was to detect critical microcrack growth between newly cast concrete and concrete damaged in a controlled manner ^[17]. Polypropylene and polyacrylonitrile fibers were added in different amounts and monitored with AE during load tests to obtain more information during the cracking process, and to optimize the composition of the mix ^[18].

Matrix damage due to fatigue loading was studied by Redjel ^[20]. An intensive increase of acoustic emission signals was related to macrocrack formation from cumulative fatigue damage due to multiplication of microcracks.

Alkali-aggregate reaction in mortar-bar specimens was reported by Niseki et al ^[21]. Various contents of alkali and reactive aggregate were tested by measuring expansions and monitoring the AE event and energy counts. The results were compared with mortar-bar specimens with normal aggregates. It was determined that reactive or deleterious aggregate could be detected within two weeks even if expansion measurements were not taken.

The influence of water and temperature on freezing damage in aerated concrete was reported by Jeong et al ^[22]. Investigation of AE characteristics, fracture mechanics J-integral tests, and SEM observations were part of the study. A large difference in AE activity and fracture toughness due to water content and temperature was found.

Drying shrinkage in concrete prisms with different mix proportions was studied with acoustic emission by Uomoto and Kato ^[23]. The specimens were measured with a length comparator and monitored with acoustic emission. AE activity was related to drying shrinkage and weight loss, after the specimens were exposed to a dry atmosphere.

Debonding of steel reinforcing bars was reported by Hawkins et al ^[24]. Uniaxial tension tests and local bond tests of bars embedded in concrete blocks were monitored with acoustic emission, together with cracks with epoxy injections. The AE signature results were found to correlate well with the predictions of a computer program which predicted the extent of internal cracking, bond stress distribution and intensity of bond stress.

Corrosion of embedded steel is another field of study ^[25]. The behavior of beams in bending tests under different loading conditions, with the reinforcement corroded by accelerated procedures, was studied. Corrosion activity was located and compared to actual corroded areas with good correlation.

An interesting laboratory experiment comparing the Japanese JIS standards vs. ASTM-RILEM standards was reported by Uomoto and Kawakami ^[26]. The finite element method was used as an analytical tool to determine stress distribution patterns under both standards. Acoustic emission was employed to provide real time detection and location of stresses for means of comparison.

2.4 TOOLS FOR ACOUSTIC EMISSION ANALYSIS

Specific equipment for concrete applications is discussed in this section, along with basic parameters used in acoustic emission tests. Also, two powerful new developments are reviewed: the “Rate Process Theory” and the “Moment Tensor Analysis”. Recently, these new techniques are being applied to AE investigations, and give the researcher the possibility to go beyond the basics and use them towards a better understanding of concrete behavior.

2.4.1 Instrumentation

Of the two basic elements of acoustic emission instrumentation, the sensor is perhaps the most sensitive to the material characteristics. In highly attenuating materials the higher frequencies of the signal are attenuated, leaving only low frequency components of the wave. The modified signals are also reduced in amplitude as they travel. This effect occurs shortly after the signals travel away from the source. If these low amplitude signals are to be captured with sensors located far from the source, in big or full-scale specimens, resonant low frequency sensors are required.

In metal testing, resonant sensors at 100-200 kHz are specified ^[2,6]. A lower frequency is desirable for research purposes in concrete, requiring resonant frequencies down to the 60 kHz range or lower. Care must be taken, however, when using sensors with resonant low frequencies that excessive ambient noise pick-up is not a problem.

For low frequency sensors, the instrumentation may have channels configured exclusively for low frequency with appropriate low-pass and high-pass filters.

2.4.2 Parameters

Well known AE parameters are used to understand concrete behavior. Signal strength and amplitude are normally used together, as both are related to the magnitude of typical events, such as cracking, where a high parametric value is representative of significant damage in the material.

The arrival time of the signal is used for source location applications. If signals are captured by the required number of sensors located on the surface, the emissions generated by a discontinuity can be located. This is done in much the same way as in earthquake foci and epicenter location in seismology. Once the source location is achieved, accurately or approximately, a detailed inspection can take place to determine the characteristics of the discontinuity, such as size and orientation.

The Kaiser effect is a powerful evaluation tool in acoustic emission testing. This effect is defined as follows: if a material is stressed and monitored with AE, the stresses removed, and then reapplied, no acoustic emission occurs until the load reaches the level corresponding to the maximum load in the previous stage. This effect is seen in many metal and composite materials. In concrete, however, it is a controversial issue. Some researchers state that the Kaiser effect is present only between 20% and 80% of the failure load ^[19]. Others

have reported that the Kaiser effect is an unreliable indicator of the loading history of concrete [14].

In metal and plastic composites testing, the Felicity effect forms part of the evaluation criteria for new and in-service pressurized and atmospheric vessels [2]. The Felicity ratio is defined as the ratio between the load at the onset of acoustic emission during a reload test and the maximum load applied to the element during the previous loading interval [8]. It has been shown that the Felicity ratio is related to the degree of deterioration or damage of the element. A value close to unity is characteristic of sound materials, while a small value (less than 1) represents the existence of degradation.

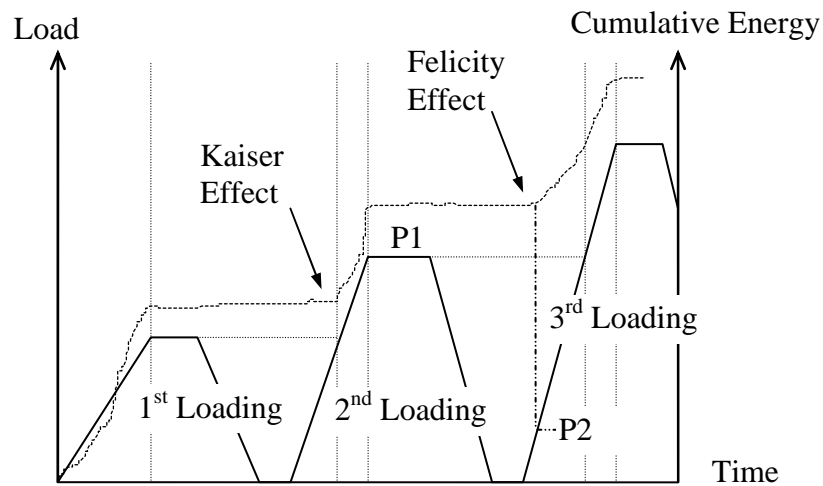


Figure 2.1 Kaiser and Felicity effect in a load/reload test.

The similarities between the two parameters described above arise from the fact that the Kaiser effect may well be represented as a special case of the Felicity ratio equal to unity. Figure 2.1 presents the Kaiser effect and Felicity ratio as obtained from a typical test. In this figure, the Kaiser effect is noted in the second loading stage. The emission continues just as the load reaches the maximum value attained at the end of the first loading.

The Felicity effect can be seen in the third loading, since the emission starts before the load reaches the maximum value of the previous loading. For this case, the Felicity ratio is $P2/P1$.

Another important technique in the evaluation of new and in-service metal and FRP structures is the Intensity analysis, which is a measure of the structural significance of a defect. This analysis provides guidance for shutdown or continued operation in in-service structures ^[27]. The two basic parameters used are the Historic Index and the Severity Index. These indices are obtained from the cumulative signal strength of a series of events in a test, and give a good indication of “changes” in the magnitude of the emission. This, in turn, can be related to significance of damage in a given structure.

2.4.3 Analytical Advances

From the research done previously, two advances are considered the most important: the “Rate Process Theory” ^[19] and the “Moment Tensor Analysis” ^[11].

THE RATE PROCESS THEORY. Its purpose is to assess damage in concrete due to microcracking by means of event rate analysis in unconfined compression tests in concrete cores.

A probability function $f(V)$ of acoustic emission occurrence from stress level $V(\%)$ to $V+dV$ is taken as:

$$f(V)dV = dN/N.$$

In this equation, N represents the cumulative hits up to stress level $V(\%)$, normalized by the failure load. The probability function $f(V)$ is assumed as the following hyperbolic function:

$$f(V) = a/V + b$$

where a and b are empirical constants. Since the discrepancy of ‘ a ’ values is considered in this theory to be a dependent form of the amount of critical microcracks, the degree of deterioration is quantitatively evaluated on the basis of the value of ‘ a ’. Increasingly negative ‘ a ’ values are a characteristic of newly cast, sound concrete, while positive ‘ a ’ values are indicative of deteriorated concrete displaying high AE activity even at very low stress levels.

This theory can be compared to a simplified intensity analysis. In this case dN/N is the slope of the cumulative hit curve, without consideration of signal strength.

Deterioration of structures studied using this theory as a valuable tool is presented by Matsuyama et al ^[19].

THE MOMENT TENSOR ANALYSIS. It has been shown that conventional AE parameter analysis such as count, hit, and amplitude measurement gives enough information to evaluate the structural integrity of metallic, FRP and concrete structures. In concrete however, the quality of the analysis will be remarkably improved if some quantitative information is available.

M. Ohtsu ^[28] has developed a moment tensor analysis based on measurement of P wave amplitudes. It is established on the basis of the elastodynamics and the dislocation theory. The AE moment tensor analysis using a SIGMA code (Simplified Green's Function for Moment Tensor Analysis) has been shown to be very effective for analyzing fracture processes of materials and structures. The most distinctive feature of this analysis is its ability to provide quantitative information of three-dimensional location of cracks, crack types, and crack orientations. This makes it possible to visualize the cracking process inside the materials.

Since the analysis requires a set of six AE waveforms recorded by six independent channels for each AE event, a fully digital, multichannel, computerized system is necessary for the task. The system must carry out simultaneous classical AE feature extraction (parametric analysis) and transient waveform analysis.

A moment tensor analysis, in essence, gives a succinct description of the incremental, steplike change in material constitution (stress geometry) that occurs

at the source that launches the AE wave. The change has to be described in all its 3-dimensional directionality, hence “TENSOR”. The magnitude of the change is expressed in units of “stress x volume “ or equivalently, “force x distance” (i.e., “MOMENT”, as in engineering beam theory and the theory of levers).

A moment tensor inversion procedure was developed by the use of only P-wave amplitude values. From the moment tensor, an eigenvalue problem is solved, and one decomposition of the eigenvalues is developed to classify the AE source as either a tensile mode crack, a mixed mode crack, or a shear mode crack.

CHAPTER 3

EXPERIMENTAL PROGRAM

3.1 INTRODUCTION

Testing of high strength prestressed concrete girders, in the Phil M. Ferguson Structural Engineering Laboratory of the University of Texas at Austin, provided the opportunity to monitor full-size specimens. Various cracking modes were monitored using existing acoustic emission equipment. The tests were part of Research Project <0-1388>, sponsored by the Texas Department of Transportation (TxDOT), to determine anchorage lengths for 6/10 in. diameter strands for pretensioned prestressed concrete beams, in three different groups having concrete strength from 5,000 to 15,000 psi.

The advantages of this particular AE program derive from the fact that a test of a full-scale specimen provides data from real structural behavior. The effects of data contamination due to wave reflection, as occurs with small laboratory specimens, are minimized. However, the low ambient noise of a laboratory does not represent field conditions where background noise is often high.

Compared to reinforced concrete, the prestress in the beam will reduce cracking significantly, promoting low signal attenuation. In addition, emission

will correspond to structurally significant damage, rather than insignificant nonstructural cracking, of the type which occurs in non-prestressed concrete.

3.2 OBJECTIVES OF THE TESTING PROGRAM

The purpose of monitoring the beam tests with acoustic emission instrumentation is to supply information on the feasibility of the technique to predict and locate cracks, and to develop a nondestructive test to provide warning of impending crack development, before they can be seen on the surface.

In the first group of tests, three basic events and zones were monitored using conventional instrumentation: a) shear-induced cracking in the web, b) flexural cracking at the region of maximum moment, and c) strand slippage at the anchorage zone.

With the aid of a Moment Tensor Analysis software donated by Physical Acoustics Corporation, a second group of tests were monitored and actual flexure cracks were analyzed and compared to the information generated by the software about source location and type of cracking.

3.3 TEST SAMPLE

The specimens tested were AASHTO Type I prestressed concrete girders with a 6.5 in. thick concrete slab cast on top in the laboratory. Figure 3.1 shows basic dimensions of the specimen.

The girders were precast at Texas Concrete, located in Victoria, Texas. The compressive strength at the time of the test varied from 5000 to 15000 psi.

Concrete for the slab was supplied by Capitol Aggregates from Austin, Texas, with a compressive strength at the time of testing of around 6000 psi. Table 3.1 shows the different concrete compressive strengths and lengths for the test beams. Since the beams consisted of two usable sections, two load tests were performed on every beam. Acoustic emission monitoring, however, took place on both sections in the four first beams only.

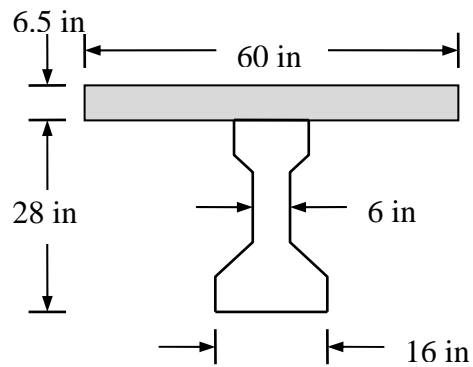


Figure 3.1 AASHTO Type I girder with slab cast on top.

Table 3.1 Characteristics of the test beams.

<i>TEST I.D.</i>	<i>BEAM LENGTH (ft)</i>	<i>CONCRETE STRENGTH @ 28 DAYS $f'c$ (psi)</i>
M0B0S and M0B0N	40	9500-11500
M0B1S and M0B1N	40	9500-11500
H0B0S and H0B0N	40	13000-15000
H0B1S and H0B1N	40	13000-15000
L4B0S	54	5000-7000
L4B1N	54	5000-7000

3.4 TEST SETUP

3.4.1 Beam Setup

Typical testing of the beams is under two point loading, with simple supports from neoprene pads supported on concrete blocks. In this way, two definite regions are defined: one of shear and one of maximum moment. A high capacity hydraulic ram mounted on a modular steel frame fixed onto a rigid test slab is used as the loading device, and a steel box girder is used to spread the load from the ram to two points on the beam.

The test setup can be seen in Figure 3.2.

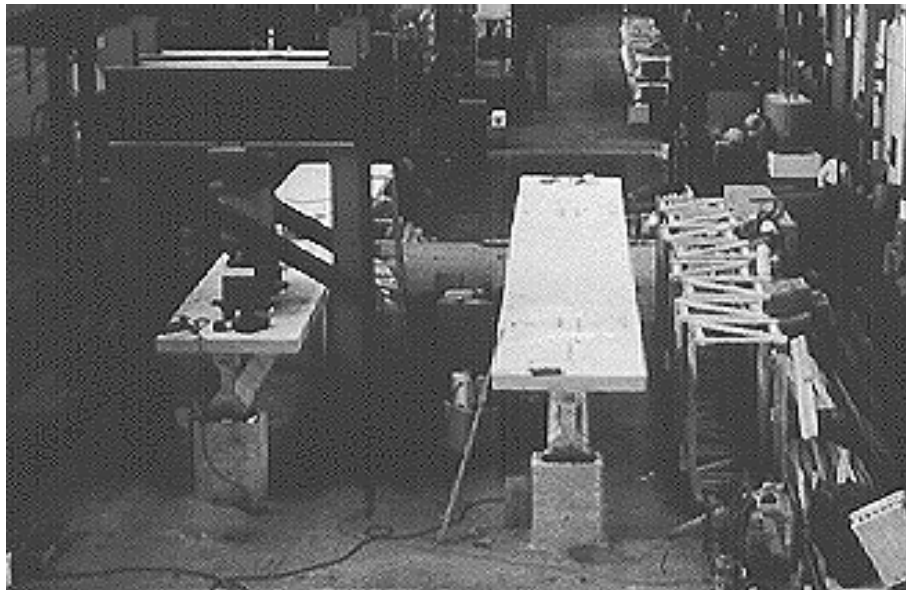


Figure 3.2 Test setup showing frame and specimen.

3.4.2 Instrumentation

SENSORS

For the first group of tests, three to seven PAC R6-I 60 kHz integral resonant sensors were used. These sensors were chosen, rather than the conventional 150 kHz sensors used in composite and steel applications, because of the greater range of the low frequency wave components. This will allow fewer sensors to be used for field applications on actual structures. The sensors were located in the flexure, shear and end regions in order to capture the characteristic events (Fig. 3.3). The channels numbers start at 13 since the equipment used had 24 channels, but only the last 12 were set up for low frequency sensors.

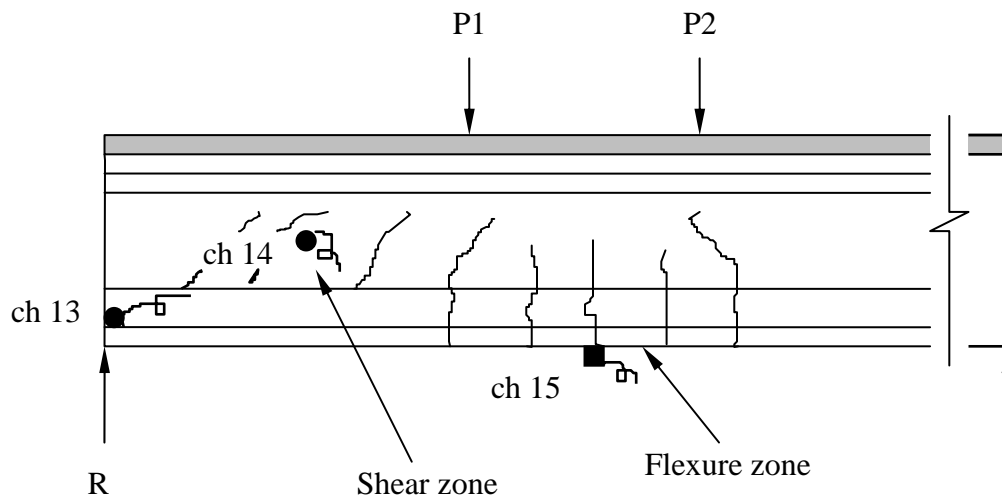


Figure 3.3 Location of sensors for group I, showing cracking zones.

The seven sensors used on the first group of tests were located as follows: one in the end zone for detection of possible strand slippage, four in a triangular array in the shear zone, and two on the bottom of the beam at a position corresponding to the load points.

Figure 3.4 shows the typical arrangement used on the seven sensor array.

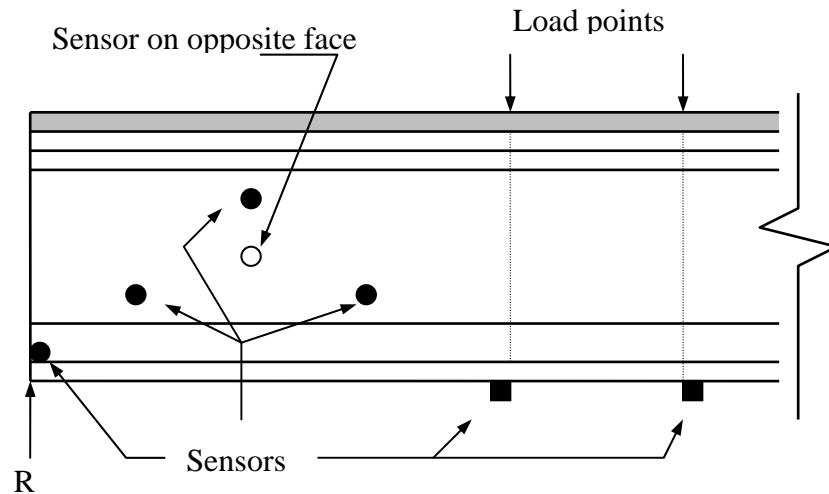


Figure 3.4 Typical sensor locations on Group I, seven sensor array.

The moment tensor analysis requires six sensors continuously monitoring. For the second group of tests, six R6-I's were concentrated in the flexure zone. Two different arrangements in two different beams were considered. For Test L4B0S (Fig. 3.5) all sensors were placed on the vertical sides of the beam, in two

groups of three on opposite faces. For Test L4B1N (Fig. 3.6) four sensors were placed on the vertical faces, and the two remaining, on the bottom of the beam at the load point lines.

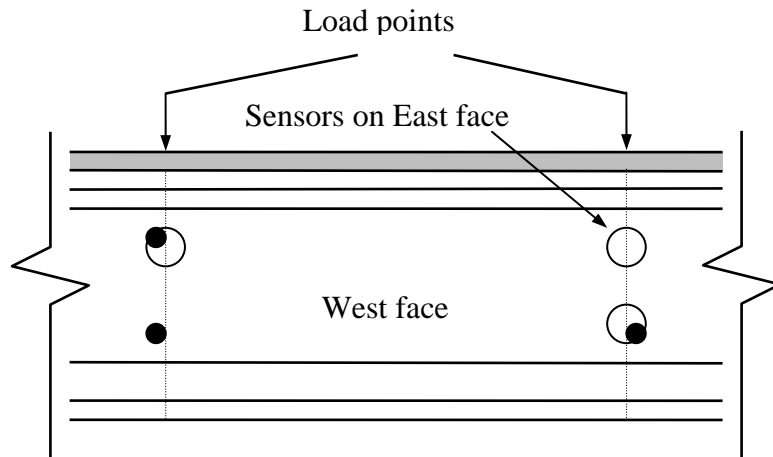


Figure 3.5 Array of sensors for Moment Tensor Analysis in Test L4B0S.

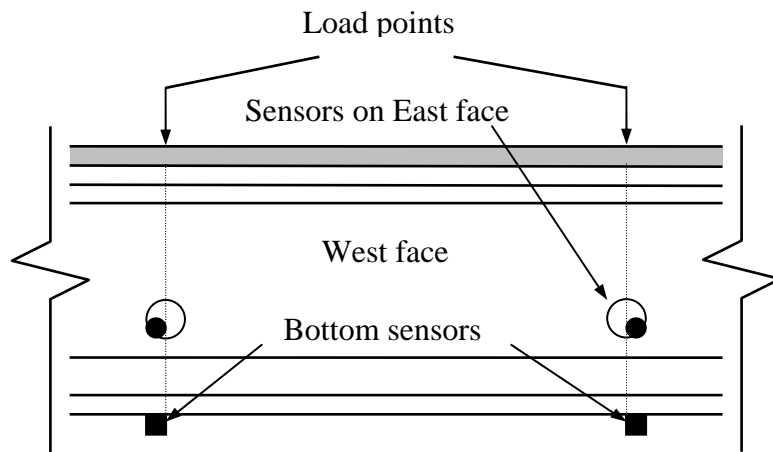


Figure 3.6 Array of sensors for Moment Tensor Analysis in Test L4B1N.

A series of trial procedures for mounting the sensors on the surface of the element were carried out. Gluing the sensor directly onto the surface did not work well because the sensor suddenly separated from the surface, and the signal did not prove reliable. Attachment of the sensor by means of plastic tape did not provide enough contact pressure and its own weight would separate it from the surface, which resulted also in a poor signal. Finally, mounting the sensors on the concrete surface was accomplished by means of a bent metal strip glued to the surface, as shown in Fig. 3.7. A bolt was used to exert contact pressure against the specimen. The coupling media used to obtain good contact between the sensor and the surface was high silicone vacuum grease from Dow Corning. This kind of attachment proved very flexible in that it allowed mounting the sensors in any desired position on the element without interfering with the crack marking process during the tests.

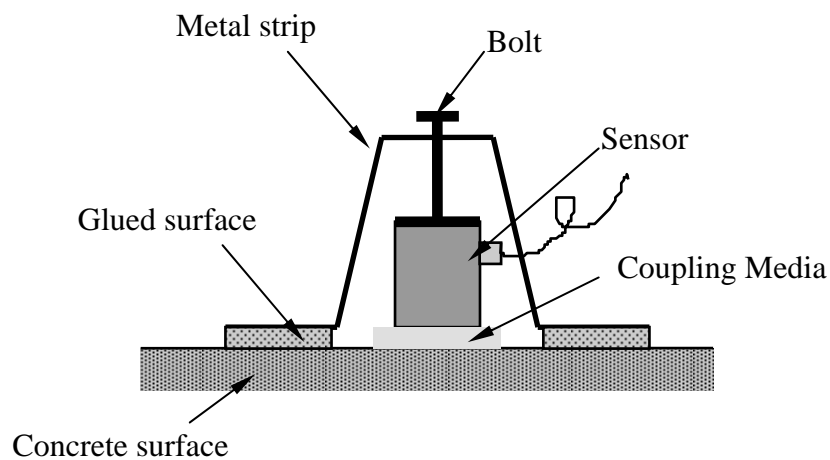


Figure 3.7 Detail of sensor mounting device.

ACOUSTIC EMISSION SYSTEMS

The instrumentation used for the first group of tests was a 24 channel MONPAC 3000 system from Physical Acoustics Corporation, with the last 12 channels calibrated for low frequency sensors. In these tests the interest was on basic parametric analysis.

For the second group of tests, a 6 channel digital system capable of waveform analysis was required. The MISTRAS 2000 system from Physical Acoustics Corporation was used for this purpose. This system is equipped with a Transient Recorder-Analyzer, necessary for Moment Tensor Analysis.

Table 3.2 gives a general overview of the equipment used in this test program for getting acoustic emission data for prestressed concrete beams.

Table 3.2 General overview of the test program.

<i>No.</i>	<i>TEST NAME</i>	<i>EQUIPMENT</i>	<i>PURPOSE</i>
1	M0B0S	MONPAC 3000 3 ch.	Basic Parameter
2	M0B0N	“	“
3	M0B1N	“	“
4	M0B1S	MONPAC 3000 7 ch.	“
5	H0B0N	“	“
6	H0B0S	“	“
7	H0B1S	“	“
8	H0B1N	“	“
9	L4B0S	MISTRAS 2000 6 ch.	Mom. Tensor Analysis
10	L4B1N	“	“

3.5 TESTING PROCEDURE

3.5.1 Calibration

The AE system has to be calibrated prior to a test, to recognize channels or sensors with low or high sensitivity and replace them. If this is not possible, they can be grouped in zones with others of similar sensitivity.

A standard calibration procedure for the sensors is specified in metal and FRP testing ^[3,6,8], using an artificial source from the lead break of a Pentel 0.3 mm mechanical pencil. However, a Pentel 0.5 mm HB lead was used on these tests because it gave a bigger pulse, more suited to concrete.

3.5.2 Data Acquisition

The beams are tested applying load in a stepwise manner. Pressure is applied to the ram by an electric or pneumatic pump until the desired load is obtained, the pump is stopped and measurements are taken of the principal parameters of the test, such as load, deflection, concrete strains, etc.

The acoustic emission monitoring of the beams takes place during the loading stage and during a two minute waiting period after the specified load is reached. Following the two minute load hold, the acoustic emission equipment is paused and a visual inspection of the beam is undertaken. After marking any cracks, the AE equipment is restarted and the cycle continues again. During the test, the AE data is displayed in real time on a monitor with various screen options. These displays give an idea of the progression of the specimen to failure. At the same time, the data is stored on magnetic disk for post-analysis.

Monitoring was performed in some cases until the beam failed. However, some tests were monitored only until the first cracks appeared on the surface, since the interest was on first crack detection.

CHAPTER 4

ANALYSIS OF RESULTS

4.1 INTRODUCTION

The analysis and presentation of results is done differently for the two types of tests. The data from the parametric tests is analyzed and presented using the program VTRANSMON (commercially available MONPAC software from Monsanto Company and Physical Acoustics Corporation [PAC]). A variety of plots such as cumulative signal strength vs. time, historic index vs. time and log duration vs. amplitude can be obtained using the mentioned software. The results of the group of tests oriented to source location and moment tensor analysis are obtained from an experimental software in two stages: a) data recording and waveform selection by the MT-TRA (Moment Tensor - Transient Recorder Analyzer) program, and b) processing of the selected waveforms by a Sigma (Simplified Green's Theorem for Moment Tensor Analysis) program from PAC. The events are located and classified following the procedure described in section 2.4.3, and compared with the actual crack pattern of the beams.

4.2 GROUP I - PARAMETRIC TESTS

This group includes the eight tests monitored with the MONPAC System. As discussed in chapter 3 the tests vary in number of sensors for each monitored zone from 1 to 4 channels in the shear zone, and 1 to 2 channels in the flexure zone.

4.2.1 Test M0B0S

For Test M0B0S three sensors/channels were used. Channel 13 was attached to the end zone, channel 14 to the shear zone and channel 15 to the flexure zone. The first observed crack was a flexure type crack at $t=2570$ sec which corresponds to a load of 221 k. In the next interval, the first shear crack was visible at the surface at $t=3832$ sec and a load of 232 k. The ultimate load for this beam was 339 k. Figure 4.1 shows the cumulative signal strength vs. time plot for the test up to 4000 sec, which is well past first cracking.

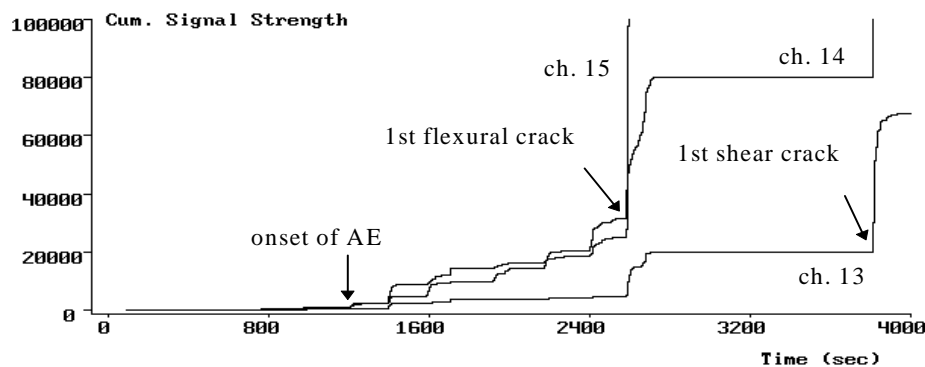


Figure 4.1 Plot of cumulative signal strength vs. time of Test M0B0S.

It can be seen that a change in the curve occurs some time before the first cracks are seen on the surface. This point is called “onset of emission” and it is believed to correspond to the start of microcracking in the material. For this test, it was determined to occur at a time $t=1200$ sec and at a load of 140 k.

A helpful analysis tool is the historic index vs. time plot. The historic index is defined as the ratio between the average signal strength of the most recent 20% of the hits and the average signal strength of all the hits. This procedure gives an indication on the change of the slope of the signal strength vs. hit number curve. A peak value on the historic index vs. time plot represents an important change in the magnitude of emission, and can normally be seen on the cumulative signal strength vs. time plot.

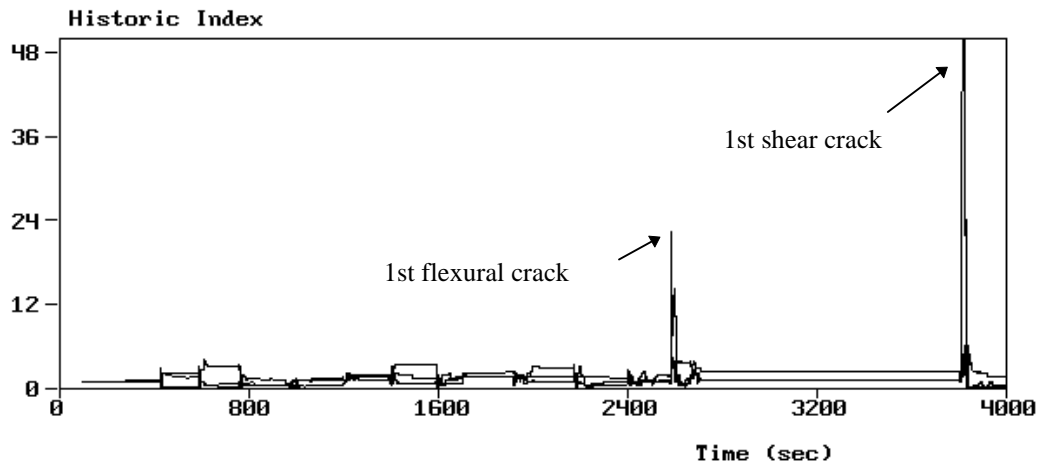


Figure 4.2a Historic index vs. time plot of Test M0B0S.

Figure 4.2a shows the historic index vs. time plot corresponding to the graph in Figure 4.1. The peak values corresponding to the to first cracks can be easily identified. Unfortunately this is not the case for the onset of emission.

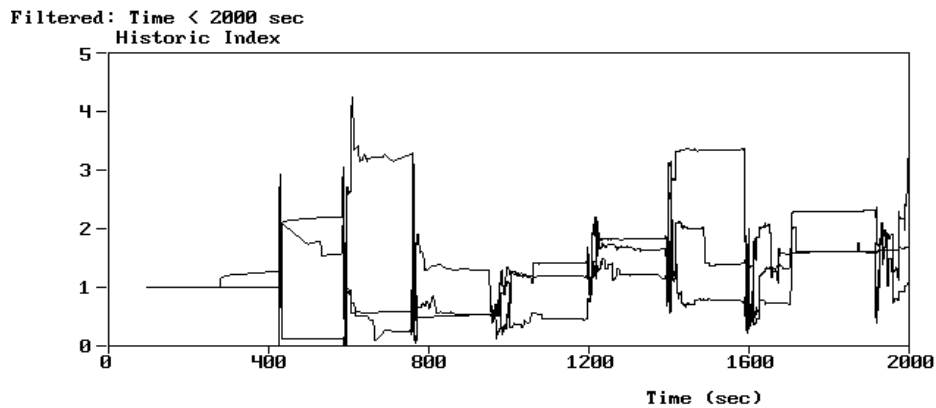


Figure 4.2b Expanded historic index vs. time plot of Test M0B0S.

An expanded graph of the historic index vs. time plot of the test up to a time $t=2000$ sec is shown on Figure 4.2b. The onset of emission at $t=1200$ sec can not be readily determined from this plot.

A very interesting graph is the log duration vs. amplitude plot. This plot, when used in metal structure testing, makes use of a zone delimited in its upper left portion corresponding to long duration, low amplitude hits characteristic of rubbing of metallic parts^[27]. Hits identified from rubbing can then be selectively removed in order to apply the required criteria to the filtered data.

Figure 4.3 shows a duration vs. amplitude plot for the test up to time $t=1200$ sec which corresponds to the onset of emission. The data is cumulative up to the specified time.

The points on the plot represent all the channels and show a typical distribution of AE hits. These are concentrated in a low amplitude, short duration band, cut off at 40 dB which is the threshold for the test, with a few hits reaching the 70-80 dB range.

Some points appear out of the band with shorter duration. These are truncated hits which are due to the dead time of the instrument when it rearms in order to prepare itself to capture a new hit after one has been processed. In this way, by the time the instrument is ready to capture a new hit, a hit might have already begun and only the last portion of it will be captured. This results in an artificially short duration hit.

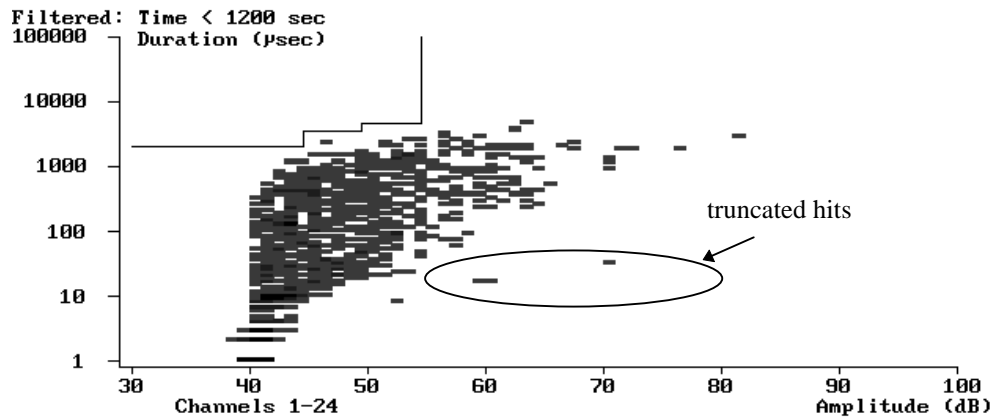


Figure 4.3 Log duration vs. amplitude plot of Test M0B0S up to $t=1200$ sec.

This problem occurs when high data rates are encountered. Development of microcracking occurs at a number of sites, and a large number of events will occur. This will result in high hit rates on nearby sensors.

Figure 4.4 presents the same graph after the onset of emission up to time $t=2000$ sec. The progress of the activity is towards higher amplitude hits as can be seen from the graph. Also a higher number of truncated hits are present which is a sign that the rate of emission is increasing.

The formation of the first crack at the surface will release a considerable amount of energy at very high rates. Figure 4.5 shows the log duration vs. amplitude plot after the first flexural crack is seen on the surface up to time $t=3000$ sec.

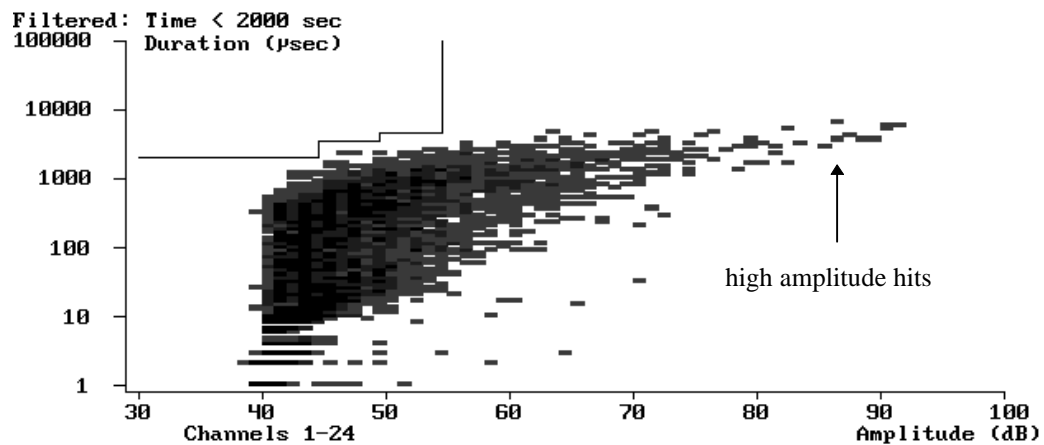


Figure 4.4 Log duration vs. amplitude plot of Test MOB0S up to $t=2000$ sec.

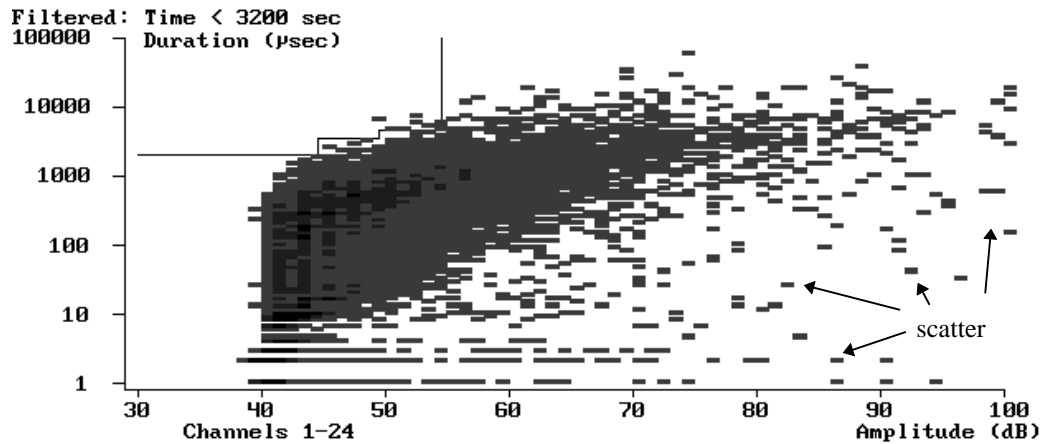


Figure 4.5 Log duration vs. amplitude plot of Test M0B0S up to $t=3200$ sec.

The considerable scatter of data shown in Figure 4.5 is due to high rates of emission associated with crack propagation, resulting in truncated and overlapping hits. Overlapping hits occur when two or more hits are considered to be part of a single event due to a high rate of emission, resulting in an artificially long hit. This phenomena is also associated with high data rates. The graph shows an increasing number of high amplitude events reaching the 100 dB mark. Microcrack growth and crack formation is associated with high energy, high amplitude hits.

4.2.2 Test M0B0N

For Test M0B0N, three channels and sensors were used in the same locations, as in the previous test, Test M0B0S. The first visible crack was of shear type and occurred at $t=2590$ sec with a load of 211 k. The ultimate load on the beam was 383 k. Figure 4.6 shows the cumulative signal strength vs. time plot for this test. The onset of emission is present at $t=1300$ sec at a load of 121 k.

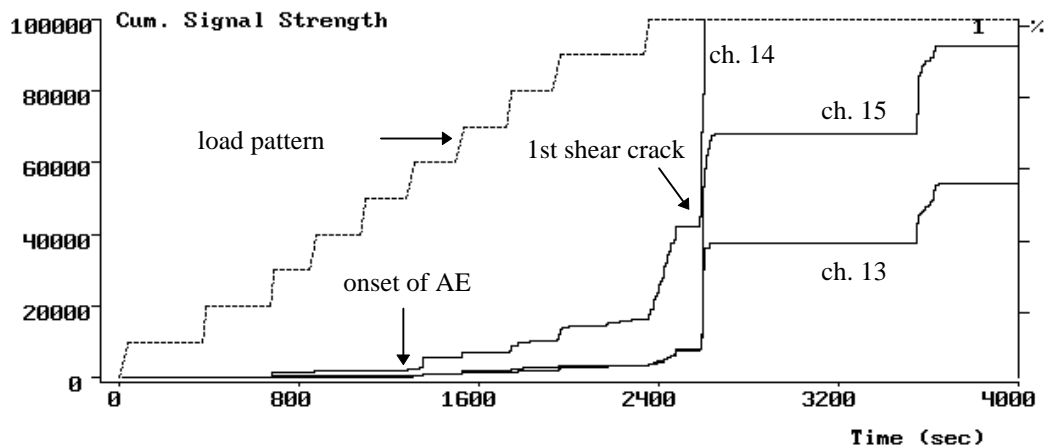


Figure 4.6 Cumulative signal strength vs. time plot of Test M0B0N.

The graph is shown up to time $t=4000$ sec, which is beyond the first cracking event. Channel 14 which was in the shear zone received the strongest signals, thus standing out from the other two.

In the same manner, the historic index vs. time plot is shown on Figure 4.7a for the test up to 4000 sec. Here, a clear difference is noted corresponding to the onset of acoustic emission. A historic index of approximately 3.6 was obtained at $t=1300$ sec. Although all three channels reported the increase in the historic index at the onset of emission, only channel 14 reached the value of 19 for the crack. This is not surprising since the shear crack occurred close to channel 14 in the shear region and in this case all the hits captured by this channel are very strong signals with little attenuation.

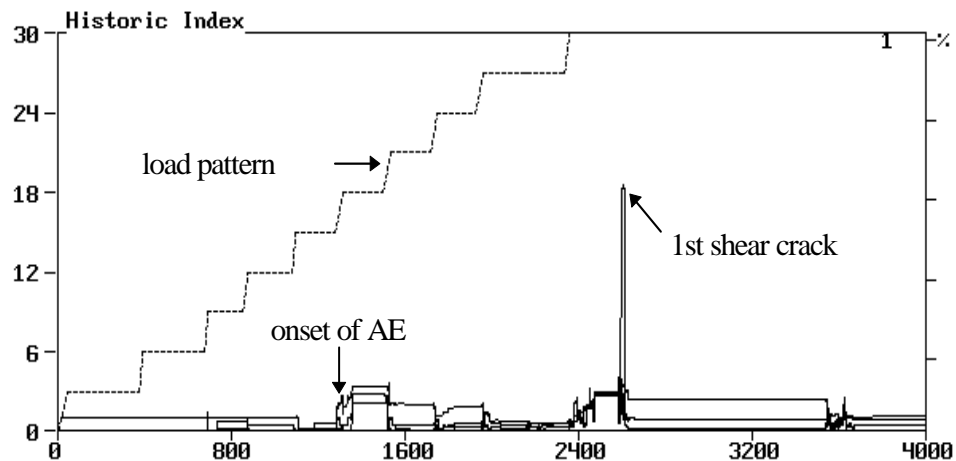


Figure 4.7a Historic index vs. time plot of Test M0B0N.

Figure 4.7b shows an expansion of the historic index vs. time plot for the test up to a time $t=2400$ sec and for a historic index range from 0 to 4. The onset of emission can be clearly identified from the plot with a value of 3.6.

The log duration vs. amplitude plots for this test up to times $t=1200$ sec, $t=2000$ sec and $t=3000$ sec, are presented in Figures 4.8, 4.9 and 4.10 respectively.

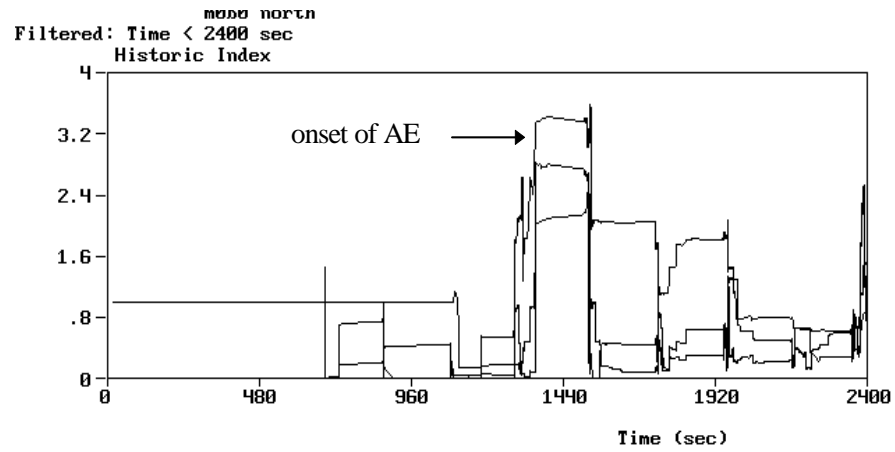


Figure 4.7b Expanded historic index vs. time plot of Test M0B0N.

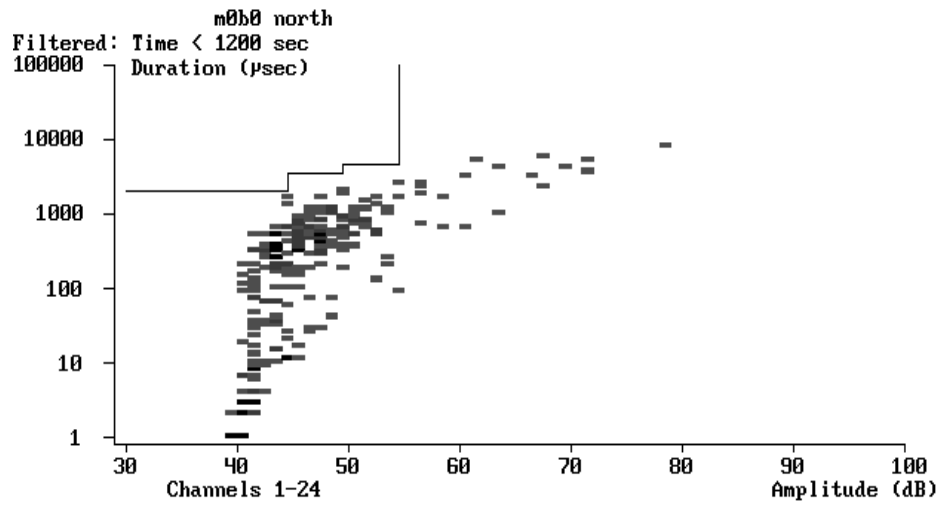


Figure 4.8 Log duration vs. amplitude plot of Test M0B0N up to t=1200 sec.

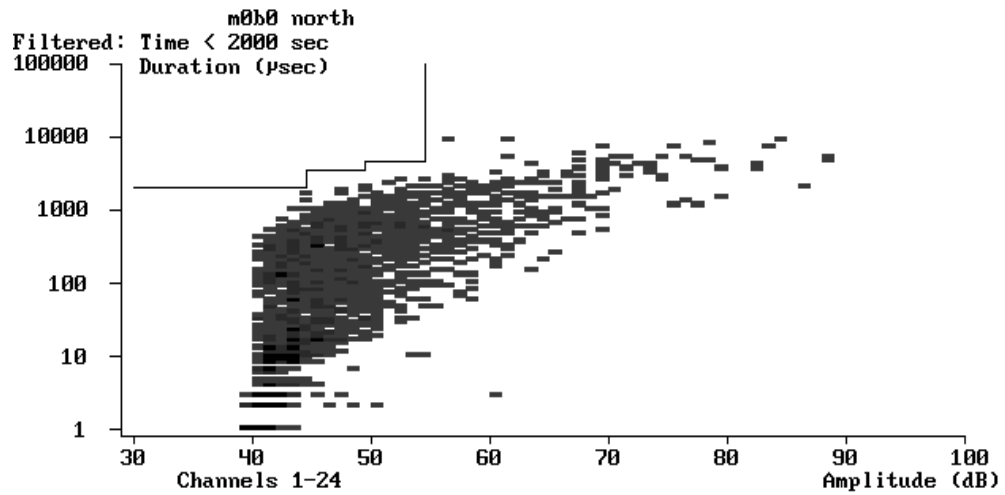


Figure 4.9 Log duration vs. amplitude plot of Test M0B0N up to t=2000 sec.

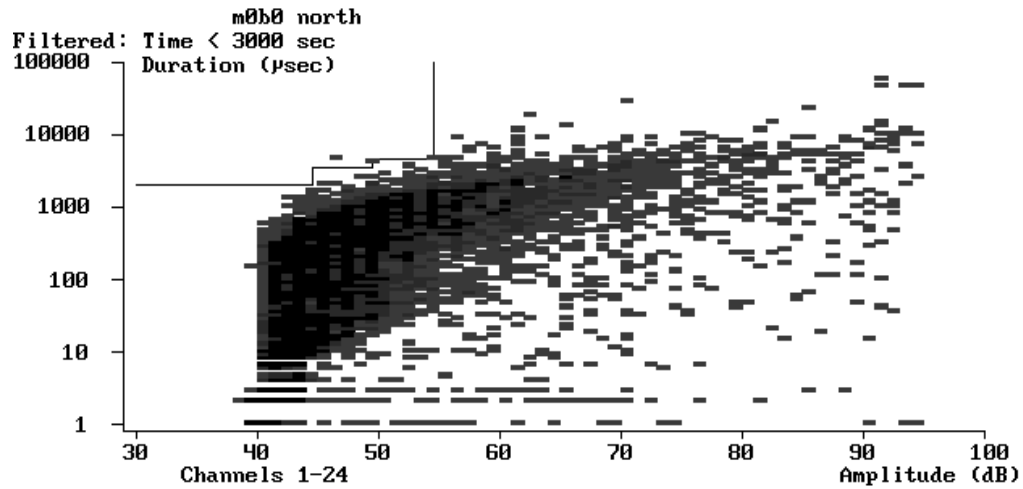


Figure 4.10 Log duration vs. amplitude plot of Test M0B0N up to t=3000 sec.

The graphs show that, after the onset of emission, high amplitude hits start to occur. Amplitudes in the range of 80 to 90 dB show between the onset of emission and the first crack stage, as well as truncated and overlapping hits. The behavior after the first crack follows the same pattern as in the first test.

4.2.3 Test M0B1N

Test M0B1N was the last beam monitored using three sensors/channels in the series of parametric tests.. The onset of emission was determined to be at t=1400 sec and at a load of 139 k. The first visible crack was of shear type and occurred at t=3086 sec with a load of 202 k (see Figure 4.11). The ultimate load resisted by the beam was 460 k.

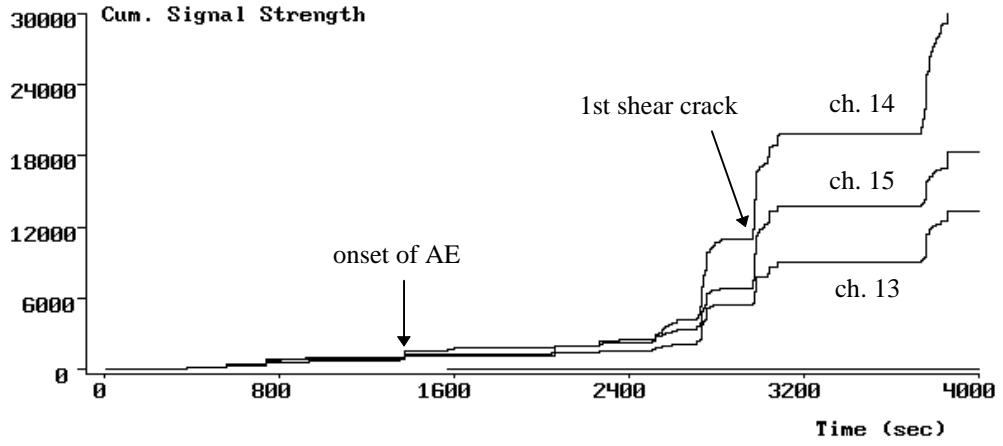


Figure 4.11 Cumulative signal strength vs. time plot of Test M0B1N.

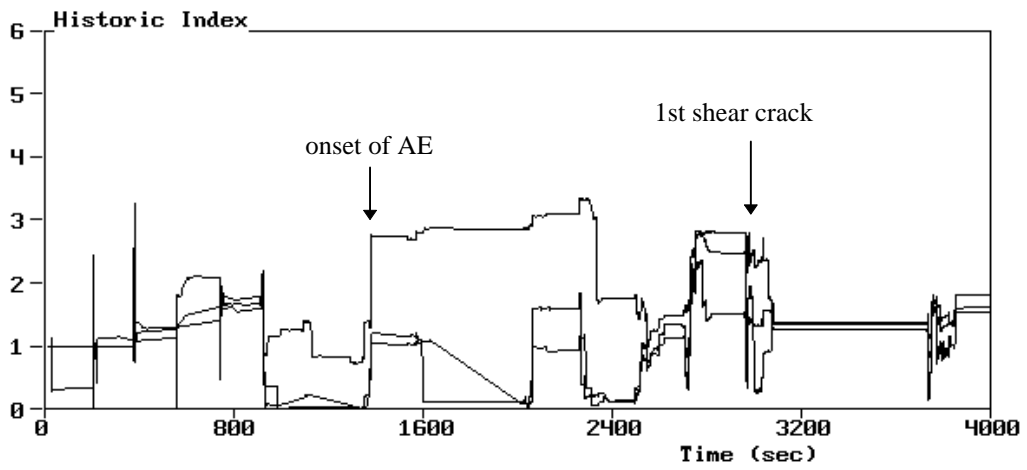


Figure 4.12 Historic index vs. time plot of Test M0B1N.

Figure 4.11 shows the cumulative signal strength vs. time plot for the test up to t=4000 sec, and Figure 4.12, the respective historic index vs. time plot.

The plots show that the first crack could have been determined to be at t=2700 sec instead of t=3086 sec. Probably, the first crack was too small to be detected in that particular load interval.

Figures 4.13 and 4.14 show log duration vs. amplitude plots for times before onset of emission and after first crack. The difference between the two graphs is marked by high amplitude hits in the 90-100 dB range, although no truncated or overlapping hits were recorded. The lack of overlapping and truncated hits might be explained by the fewer total number of hits, when compared to the other tests, which resulted in lower hit rates.

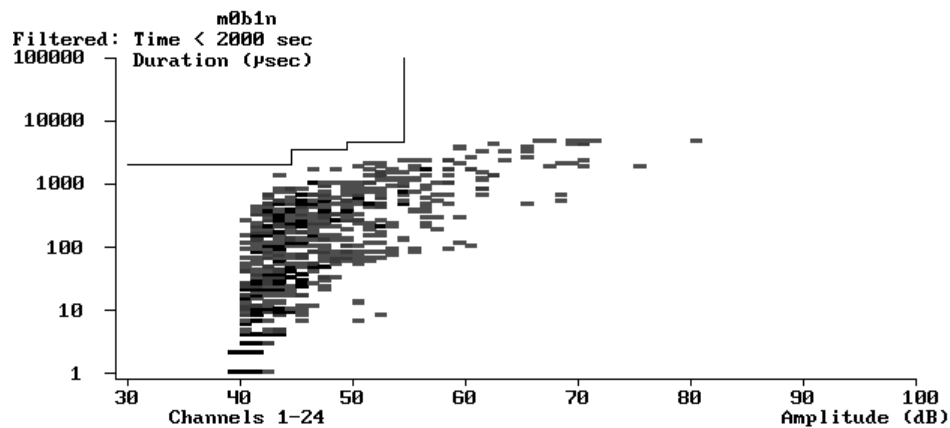


Figure 4.13 Log duration vs. amplitude plot of Test M0B1N up to t=2000 sec.

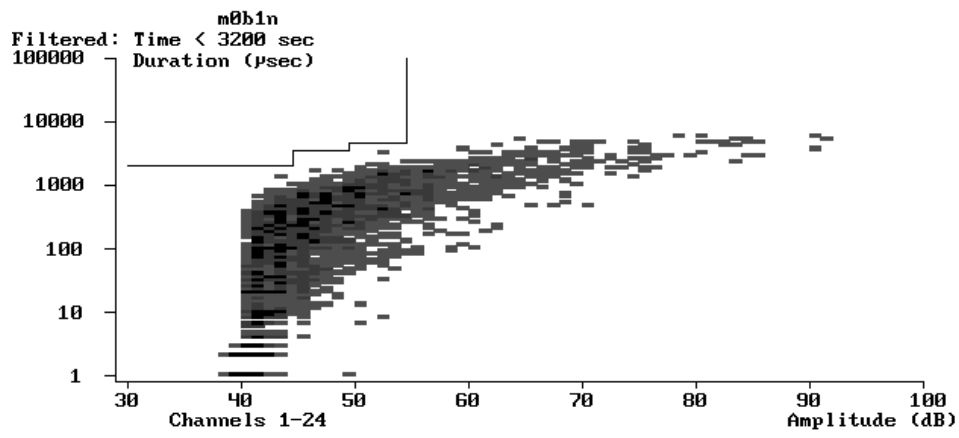


Figure 4.14 Log duration vs. amplitude plot of Test M0B1N up to t=3200 sec.

4.2.4 Test M0B1S

Test M0B1S was the first of the group of parametric tests to use seven sensors/channels for more sensitivity. The sensors were distributed in the following manner: one in the end zone, four in the shear zone, and two in the flexure zone.

Figure 4.15 shows the cumulative signal strength vs. time plot for the test past first cracking up to $t=4000$ sec.

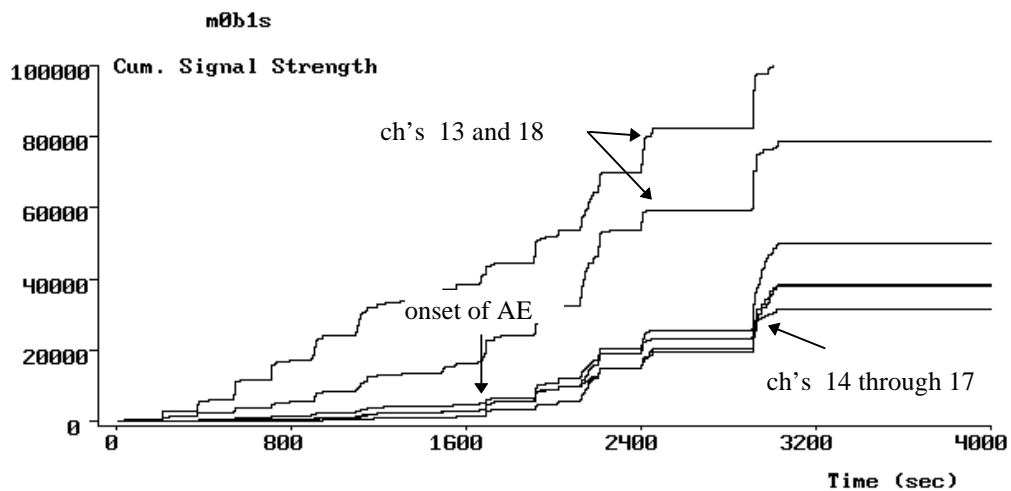


Figure 4.15 Cumulative signal strength vs. time plot of Test M0B1S.

The graph shows that two sensors, channels 13 and 18, captured more energy than the rest. Channel 13 was attached to the end zone and channel 18 to the bottom of the slab in the flexural zone. As can be seen from Figure 4.15, these sensors detected emission from the beginning of the test, with the emission

pattern recorded by the other sensors superimposed on a steady rate of background emission, or background noise. This background noise was not recorded on channels 14 through 17 because they had relative lower sensitivity, detected after the test with pencil breaks.

Although valid information was obtained from this test, the use of this particular sensors was discontinued, and they were returned to the manufacturer for repair.

During this test, the onset of acoustic emission was detected at $t=1680$ sec and at a load of 171 k. The first shear crack was visible at the surface at $t=2910$ sec and at a load of 211 k. The ultimate load for the beam was 474 k.

Figure 4.16 shows the historic index vs. time plot for the test. In this figure, the peak corresponding to the onset of acoustic emission can be identified as the first peak reaching a historic index value of 4.0. The peak related to the first observed shear crack is also seen in the graph.

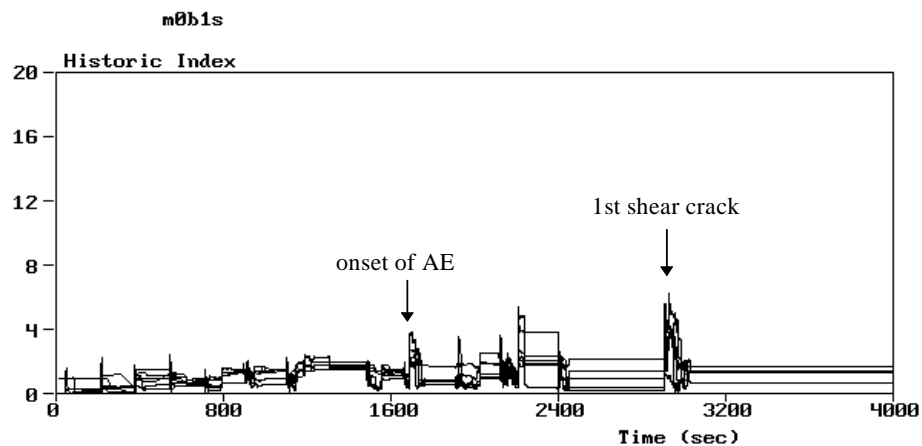


Figure 4.16 Historic index vs. time plot of Test M0B1S.

The effect of channel sensitivity and background noise can be appreciated in Figures 4.17 through 4.20. Figure 4.17 shows the log duration vs. amplitude plot up to $t=1200$ sec for all the sensors. Even though the onset of emission has not yet occurred, high amplitude hits and truncated and overlapping hits are present. In Figure 4.18 only channels 14 through 17 are considered. Now, a comparison can be made, and the effects of channels with relative higher sensitivity in areas of lower interest, or background noise, can be minimized.

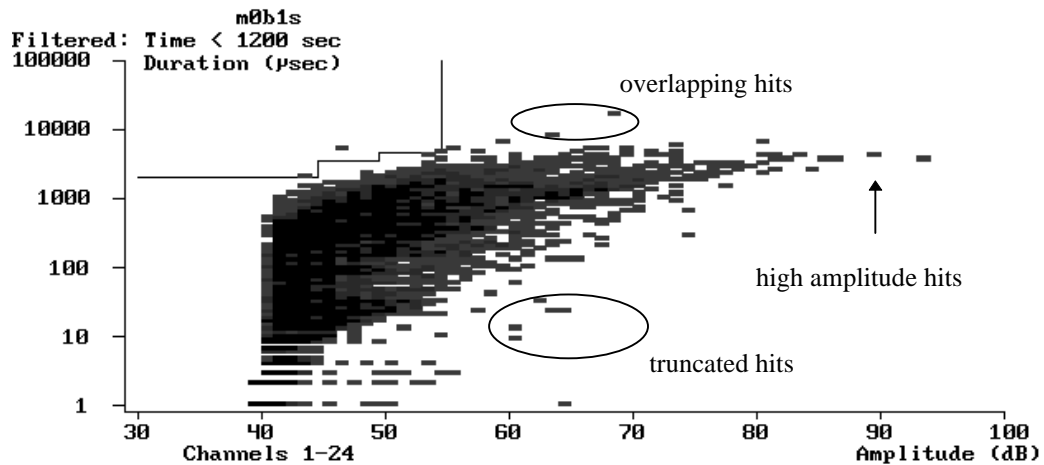


Figure 4.17 Log duration vs. amplitude plot of Test MOB1S up to $t=1200$ sec.

Figure 4.19 shows the log duration vs. amplitude plot after the onset of emission at $t=2000$ sec and before the first shear crack for the group of channels 14 through 17. The truncated and high amplitude hits are noticed on this figure.

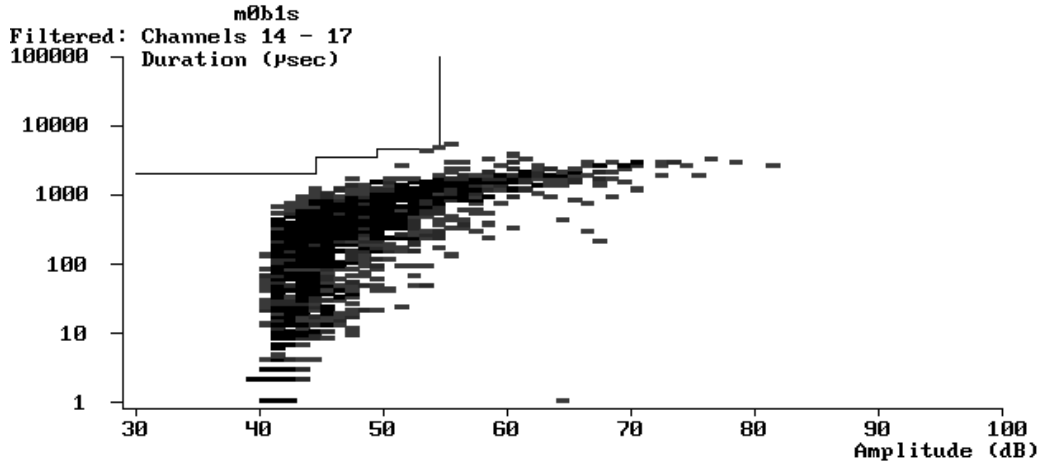


Figure 4.18 Log duration vs. amplitude plot of Test M0B1S, ch.: 14-17, t=1200 sec.

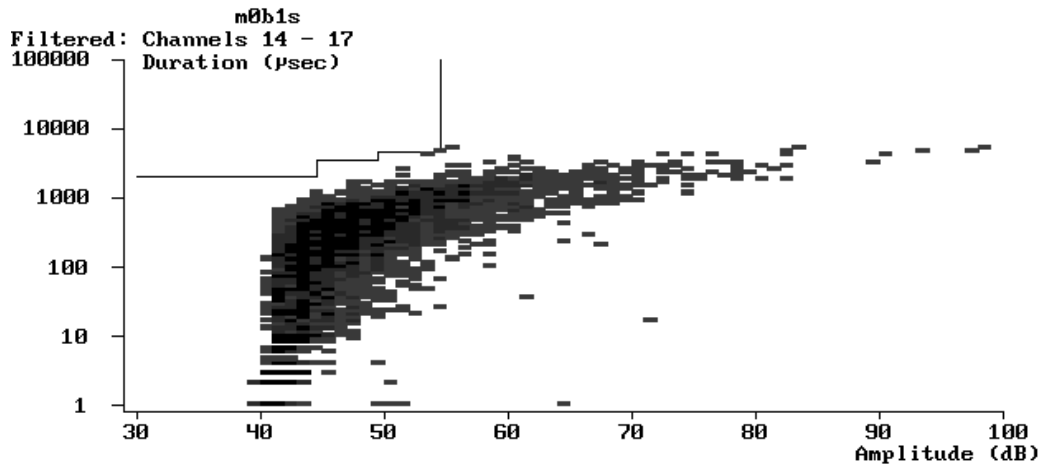


Figure 4.19 Log duration vs. amplitude plot of Test M0B1S, ch.: 14-17, t=2000 sec.

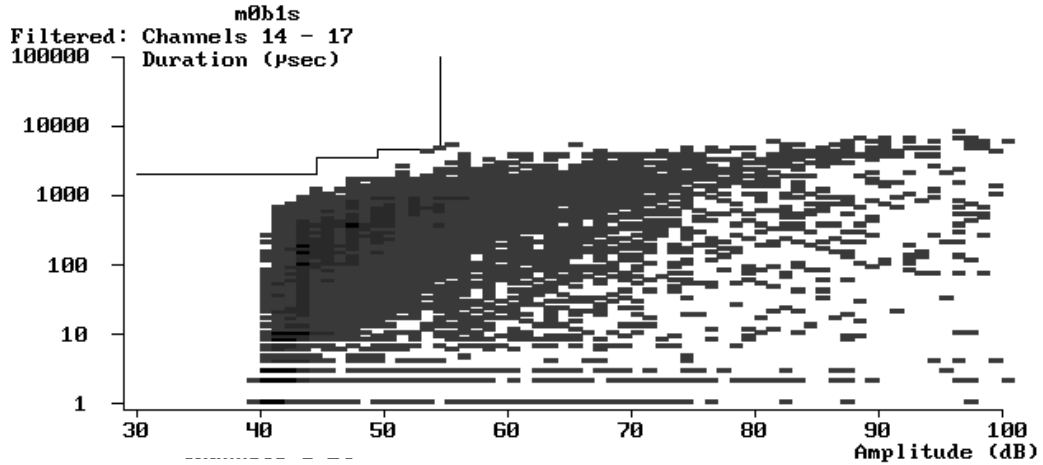


Figure 4.20 Log duration vs. amplitude plot of Test M0B1S, ch.: 14-17, t=3200 sec.

Figure 4.20 shows the log duration vs. amplitude plot for the test including only channels 14 through 17 after the first crack. It can be noticed the scatter due to truncated hits and very high amplitude events in the 90-100 dB range typical of the cracking stage.

4.2.5 Test H0B0N

The monitoring of Test H0B0N started on the third load interval, when the beam already had a force of 40 k applied. The onset of AE is localized at t=1200 sec and at a load of 161 k. First cracking corresponds to two cracks: a shear

crack, plus a flexure crack, at $t=2520$ sec and at a load of 222 k (see Figure 4.21). The ultimate load for the beam was 341 k.

Figure 4.21 shows the cumulative signal strength vs. time plot for the test. Figures 4.22a and 4.22b show normal and expanded historic index vs. time plots for the test. The onset of acoustic emission is easily detected in these graphs.

Figures 4.23 through 4.25 show log duration vs. amplitude plots at times $t=1000$ sec, $t=1800$ sec, and $t=2600$ sec.

The behavior is similar to that encountered in other tests. High amplitude hits and truncated and overlapping hits are present after the first crack is seen on the surface of the beam.

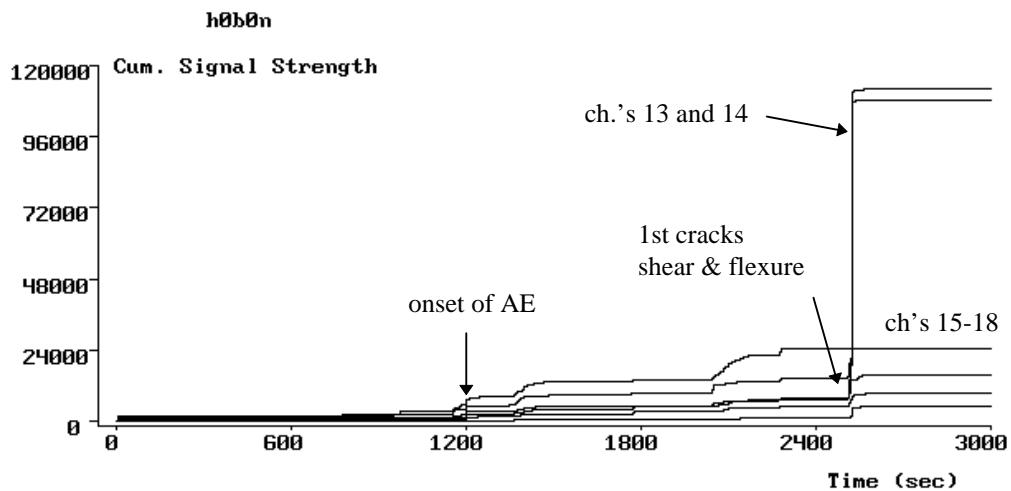


Figure 4.21 Cumulative signal strength vs. time plot of Test H0B0N.

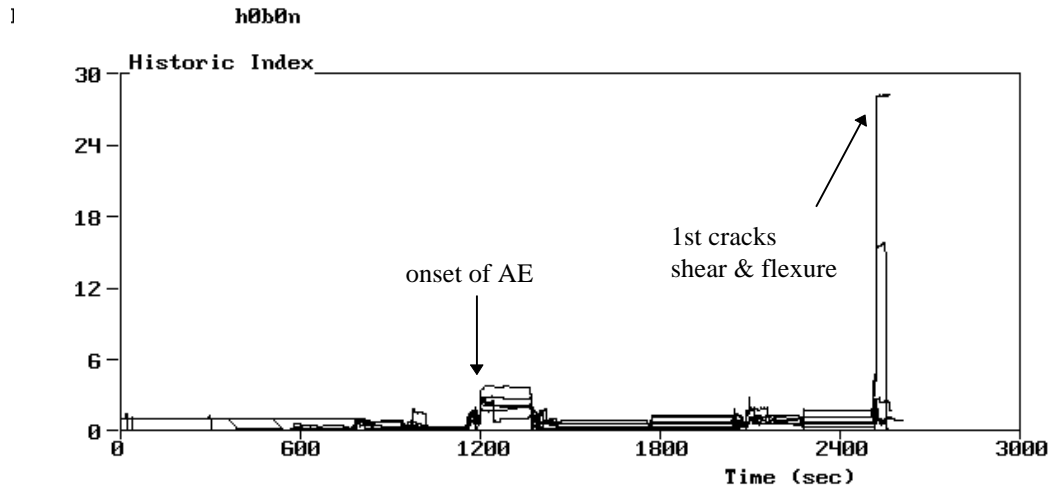


Figure 4.22a Historic index vs. time plot of Test H0B0N.

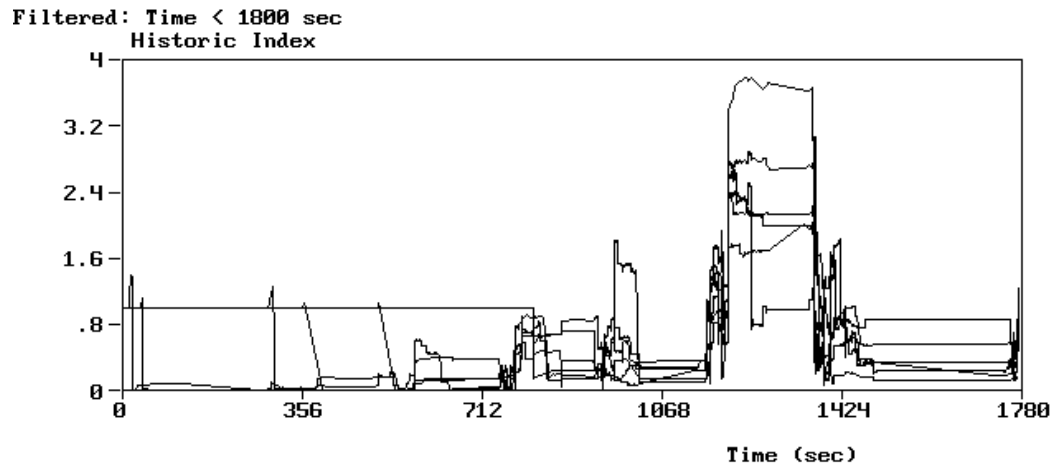


Figure 4.22b Expanded historic index vs. time plot of Test H0B0N.

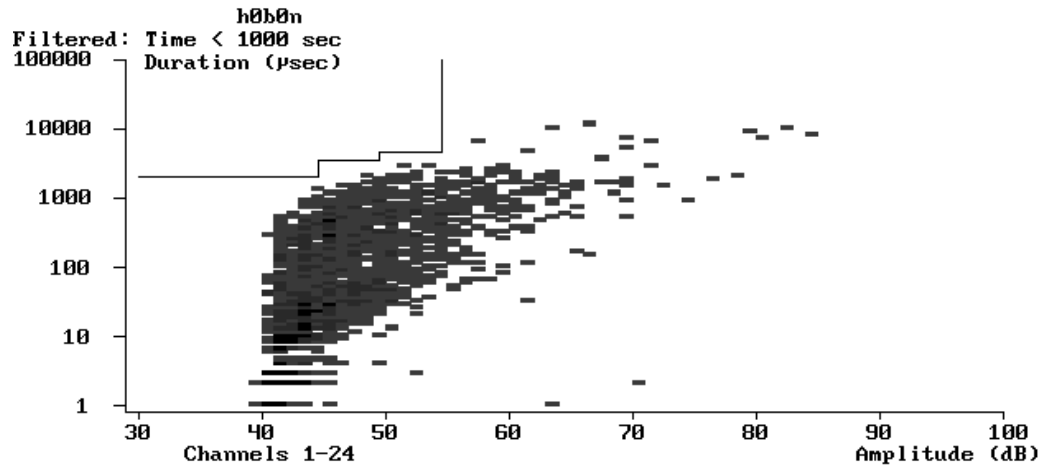


Figure 4.23 Log duration vs. amplitude plot of Test H0B0N up to t=1000 sec.

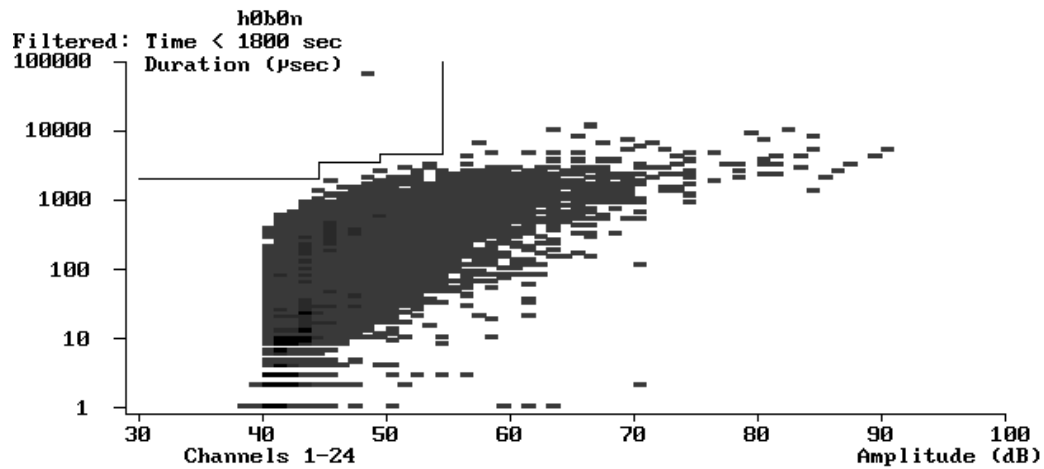


Figure 4.24 Log duration vs. amplitude plot of Test H0B0N up to t=1800 sec.

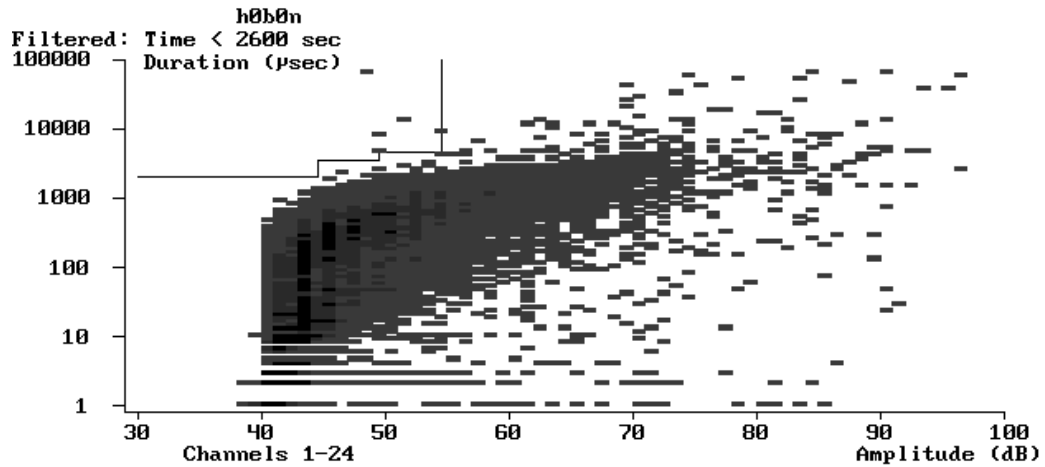


Figure 4.25 Log duration vs. amplitude plot of Test H0B0N up to t=2600 sec.

4.2.6 Test H0B0S

For Test H0B0S seven channels were used, divided in two groups. The first group consists of four channels in the shear zone (ch's 14 through 17), plus one in the end zone (ch. 13). The second group consists of two channels in the flexure zone (ch's 19 and 20), and are shown on a separate display.

Figures 4.26 and 4.27 show cumulative signal strength vs. time plots for the two groups of channels.

Figures 4.28 and 4.29 show the corresponding historic index vs. time plots for Test H0B0S.

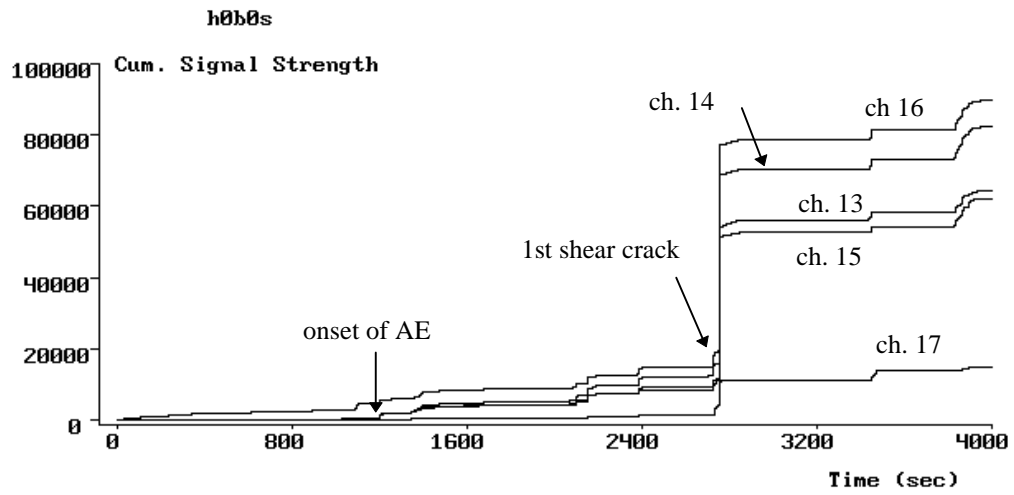


Figure 4.26 Cumulative signal strength vs. time plot, Test H0B0S, ch.: 13-17.

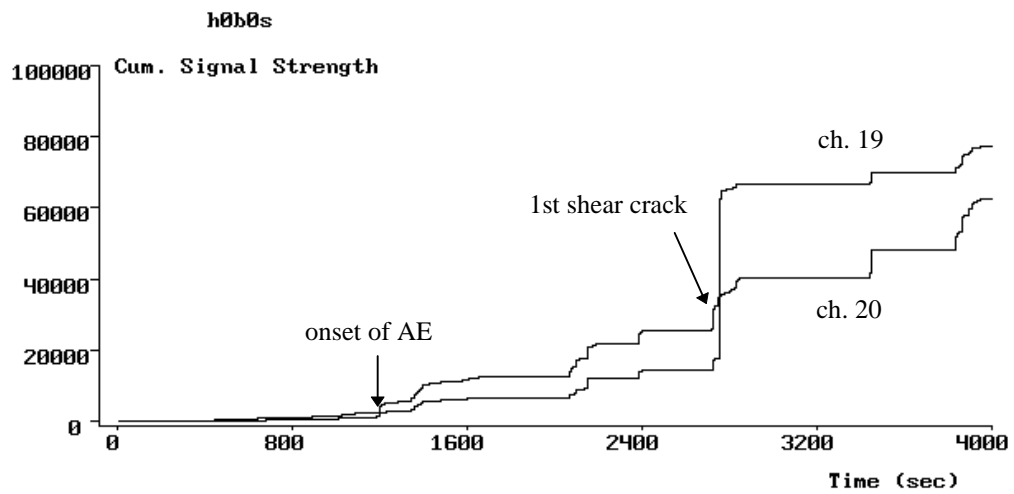


Figure 4.27 Cumulative signal strength vs. time plot, Test H0B0S, ch.: 19-20.

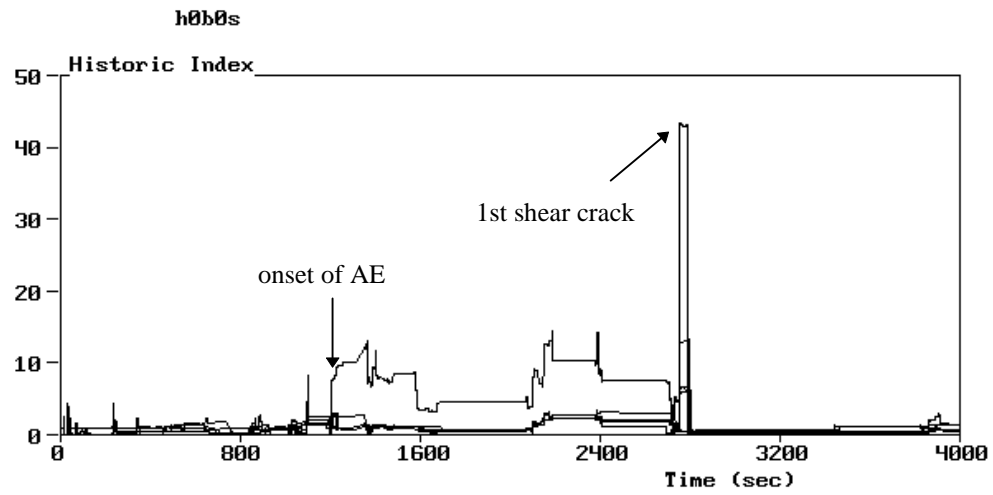


Figure 4.28 Historic index vs. time plot of Test H0B0S, ch.: 13-17.

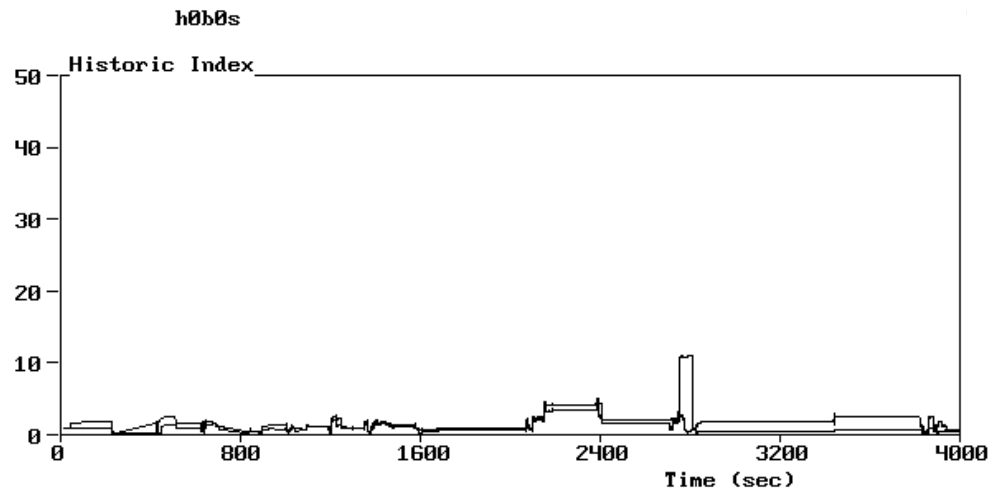


Figure 4.29 Historic index vs. time plot of Test H0B0S, ch.: 19-20.

The onset of emission occurs at $t=1200$ sec, which corresponds to a load of 144 k. The first crack seen on the surface was a shear crack at $t=2730$ sec at a load of 203 k (see Figures 4.26 and 4.27). The ultimate load resisted by the beam was 391 k.

The historic index vs. time plots show lower activity in the flexure zone channels (Figure 4.29). This is expected since the first crack appeared in the shear zone (Figure 4.28).

Figures 4.30 through 4.32 show log duration vs. amplitude plots including all the channels for the test up to times $t=900$ sec, $t=2000$ sec and $t=3200$ sec. Although the initial distribution appears different from the other tests, the basic behavior is also seen on these graphs.

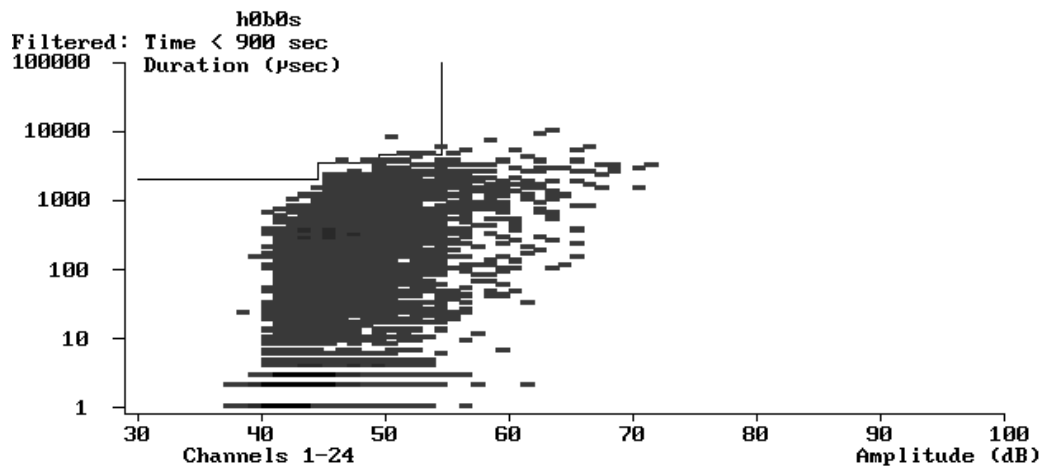


Figure 4.30 Log duration vs. amplitude plot of Test H0B0S up to $t=900$ sec.

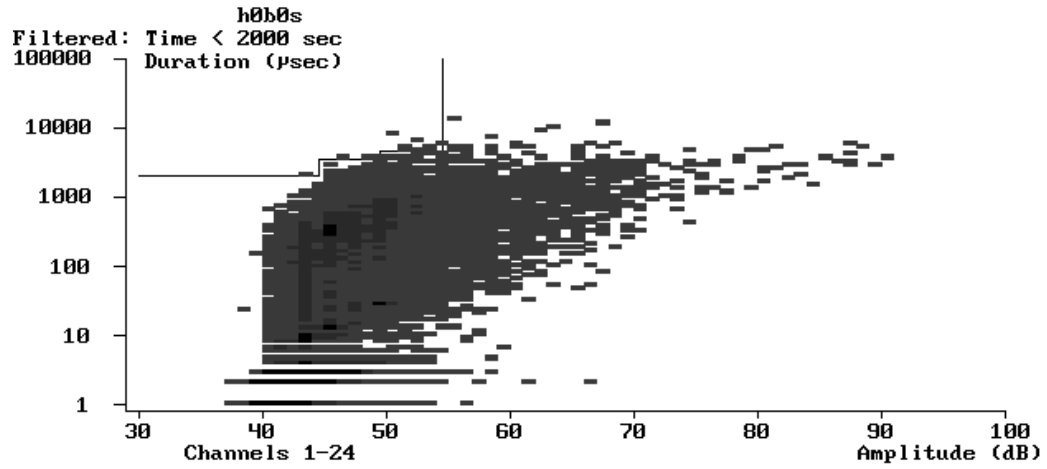


Figure 4.31 Log duration vs. amplitude plot of Test H0B0S up to t=2000 sec.

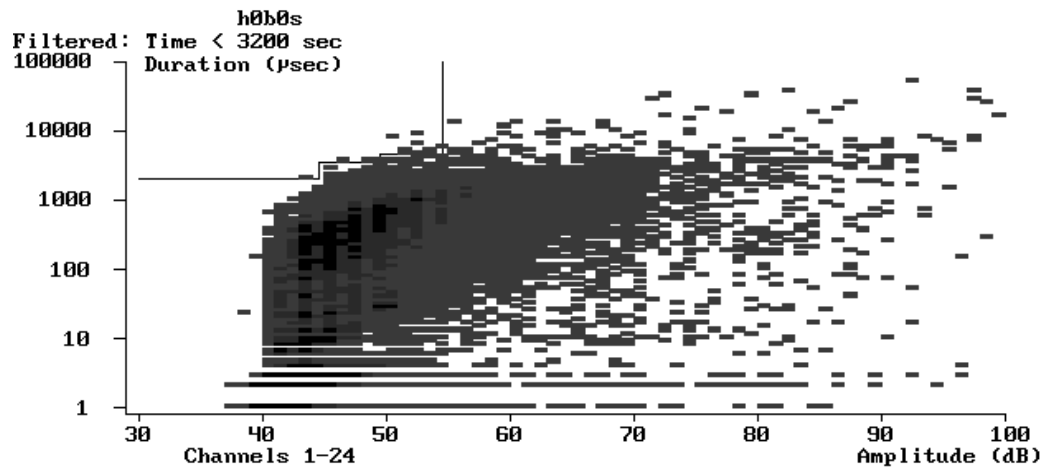


Figure 4.32 Log duration vs. amplitude plot of Test H0B0S up to t=3200 sec.

4.2.7 Test H0B1S

For Test H0B1S the channels were also divided into two groups as in the previous tests. The onset of emission was detected at $t=800$ sec at a load of 141 k. The first shear crack appeared at the surface at $t=2335$ sec and at a load of 201 k (see Figure 4.33). The ultimate load resisted by the beam was 467 k.

Figures 4.33 and 4.34 show cumulative signal strength vs. time plots for the test for the two groups: a) channels 13 through 17 in the end and shear zone, and b) channels 19 and 20 in the flexure zone.

Although the cumulative energy at the time of cracking was low, the onset of emission can still be detected. A clear change in the slope occurs at $t=800$ sec. This is reflected in Figures 4.35a, 4.35b and 4.36 which show the corresponding historic index vs. time plots for the test, where a significant value of 4 is reached at the onset of emission.

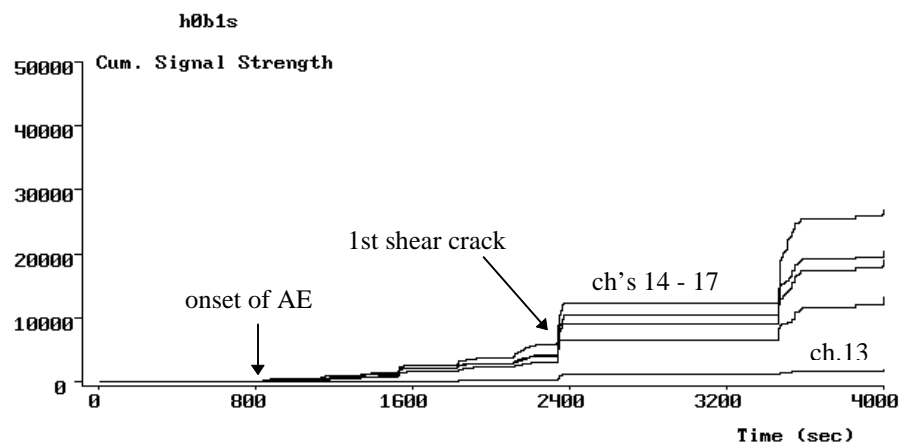


Figure 4.33 Cumulative signal strength vs. time plot, Test H0B1S, ch.: 13-17.

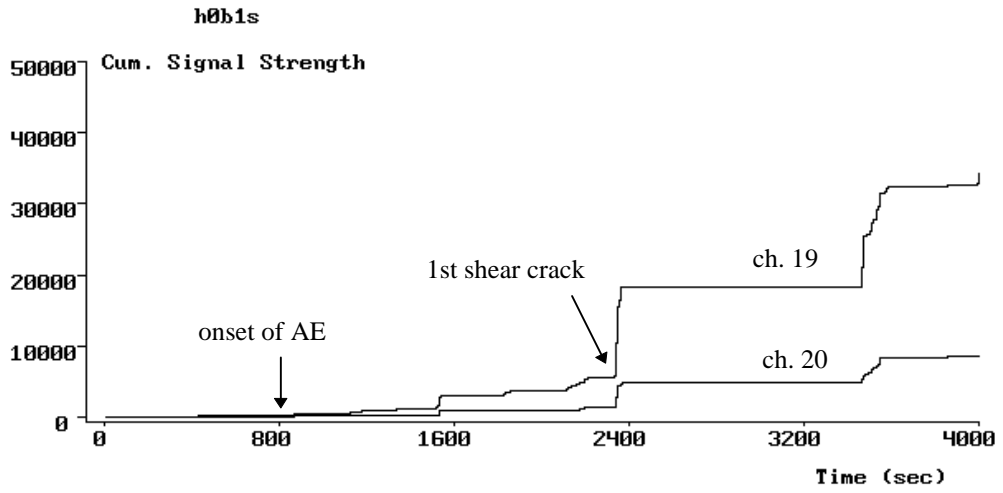


Figure 4.34 Cumulative signal strength vs. time plot, Test H0B1S, ch.: 19-20.

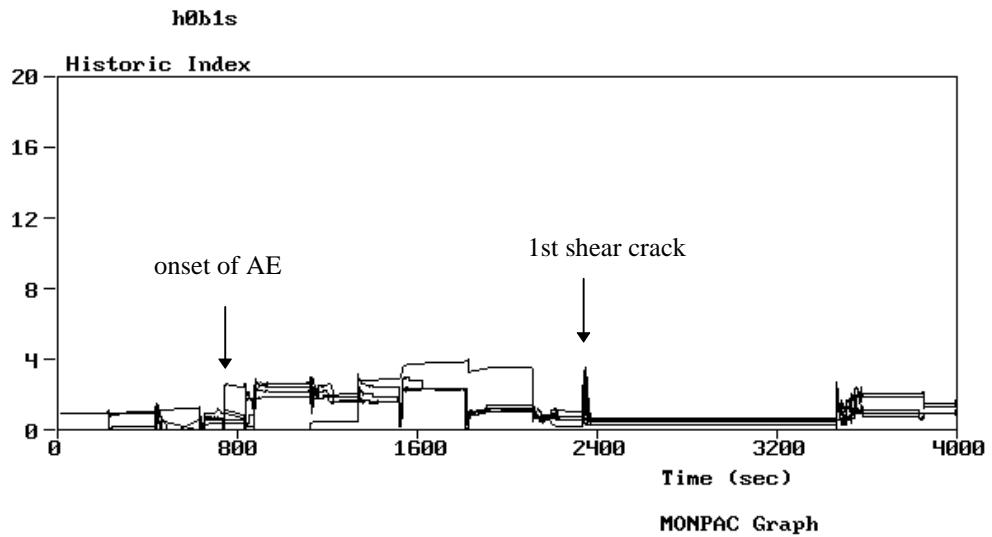


Figure 4.35a Historic index vs. time plot of Test H0B1S, ch.: 13-17.

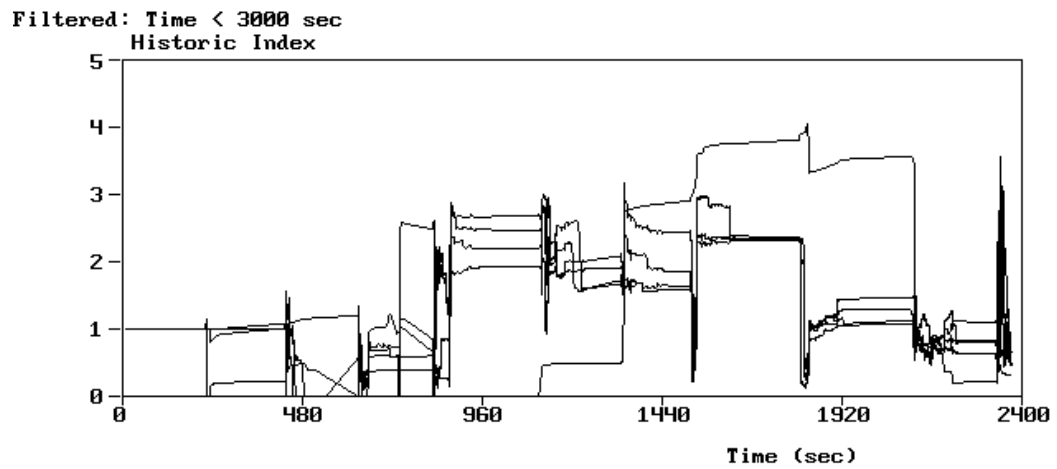


Figure 4.35b Expanded historic index vs. time plot, Test H0B1S, ch.: 13-17.

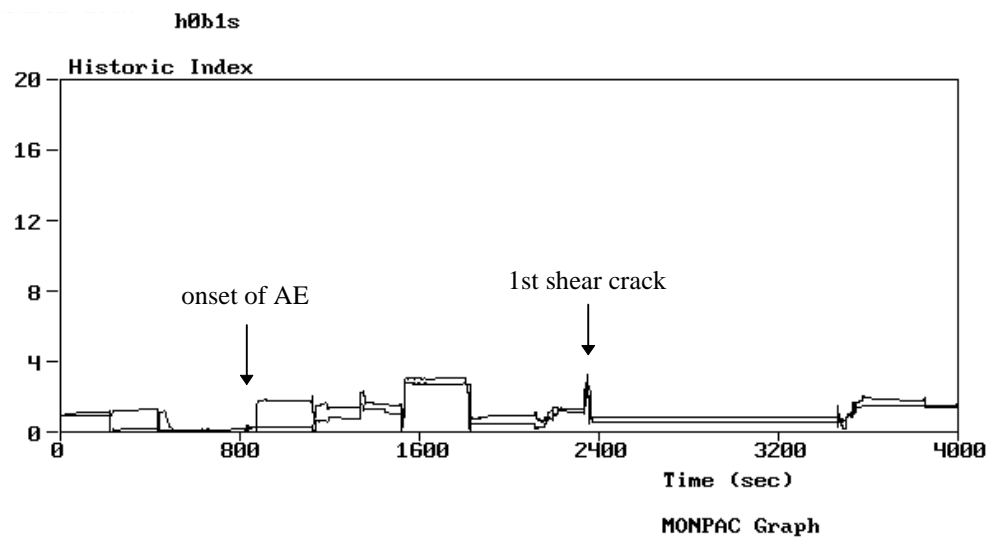


Figure 4.36 Historic index vs. time plot of Test H0B1S, ch.: 19-20.

Log duration vs. amplitude plots are shown on Figures 4.37 through 4.39 for times $t=800$ sec, $t=2000$ sec and $t=3000$ sec. The pattern is the same as was observed in all the tests.

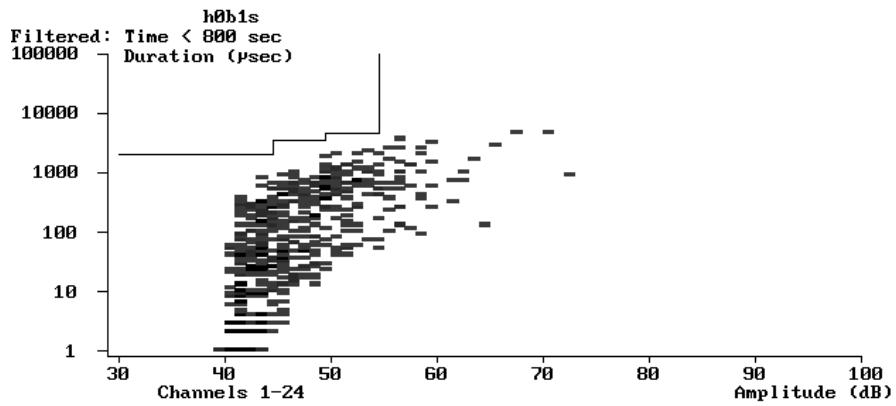


Figure 4.37 Log duration vs. amplitude plot of Test H0B1S up to $t=800$ sec.

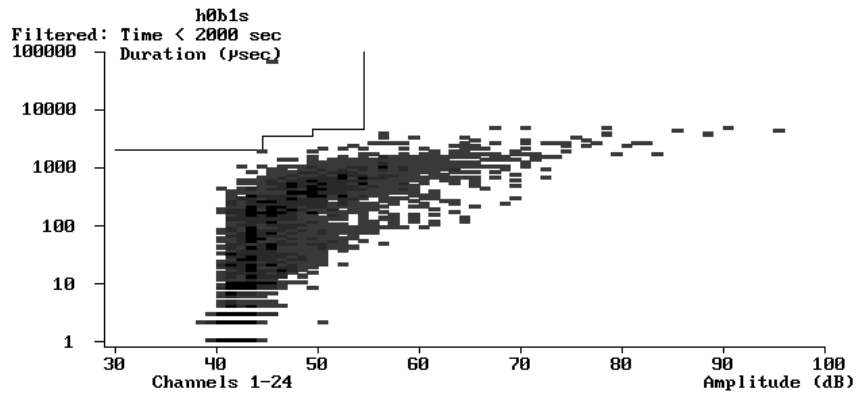


Figure 4.38 Log duration vs. amplitude plot of Test H0B1S up to $t=2000$ sec.

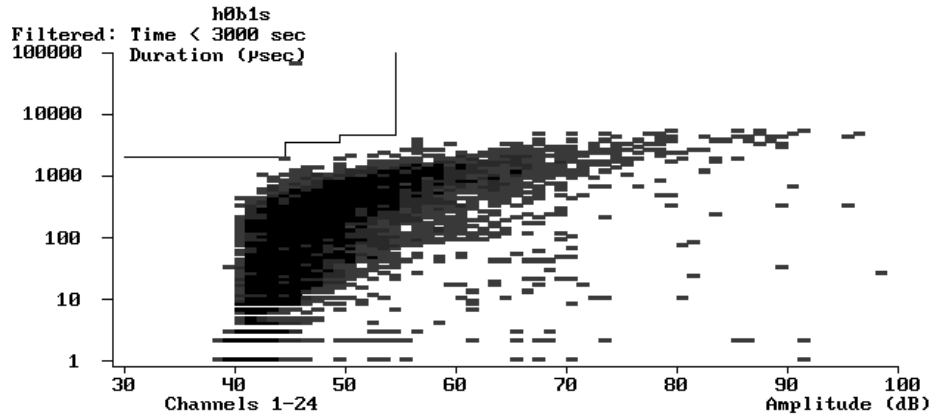


Figure 4.39 Log duration vs. amplitude plot of Test H0B1S up to $t=3000$ sec.

4.2.8 Test H0B1N

The sensors for Test H0B1N were arranged in two groups, in the same manner as in the previous test. Figures 4.40 and 4.41 show cumulative signal strength vs. time plots for the two groups of channels. Figure 4.42 shows the historic index vs. time plot for the first group. The first visible crack was of shear type and occurred at $t=2350$ sec with a loading of 210 k. The capacity of the beam was 472 k. For this test the onset of acoustic emission was determined at $t=1000$ sec with a loading of 141 k. In this case, the onset of emission was determined from the cumulative signal strength vs. time plot, since it was not possible to define it from the historic index plot.

Figures 4.43 through 4.45 present log duration vs. amplitude plots for Test H0B1N, at times $t=800$ sec, $t=1800$ sec and $t=2400$ sec, respectively. These figures show similar behavior compared to previous tests.

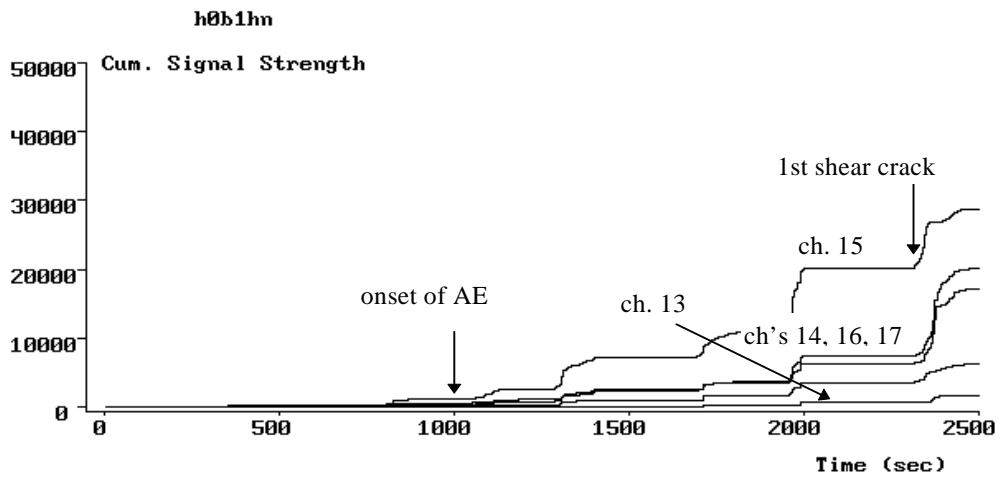


Figure 4.40 Cumulative signal strength vs. time plot, Test H0B1N, ch: 13-17.

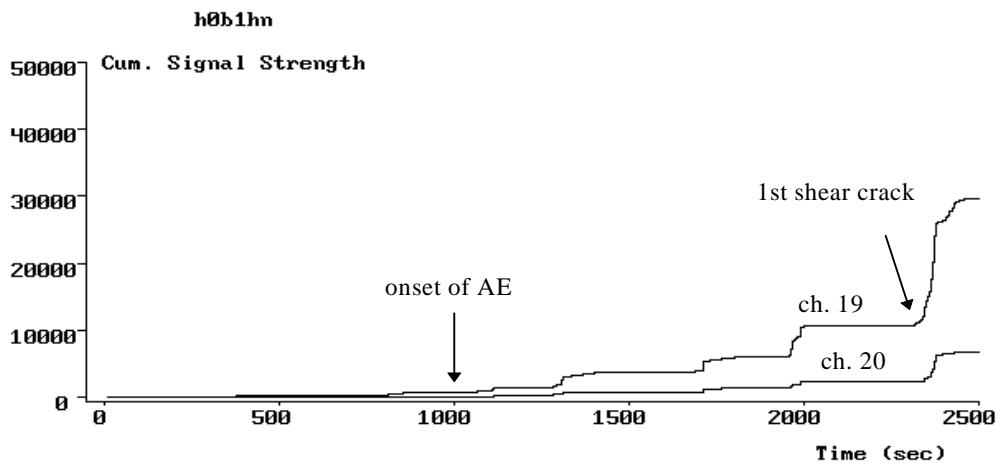


Figure 4.41 Cumulative signal strength vs. time plot, Test H0B1N, ch.: 19-20.

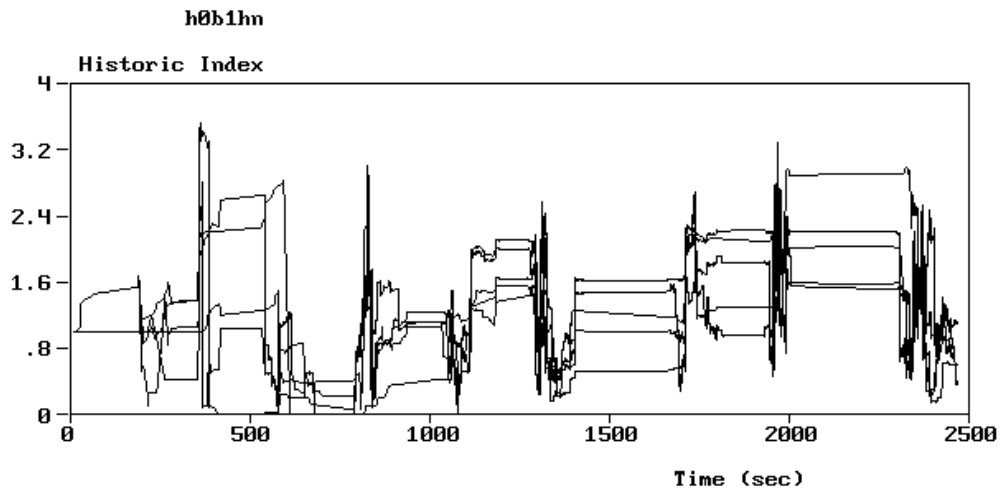


Figure 4.42 Historic index vs. time plot of Test H0B1N, ch.: 13-17.

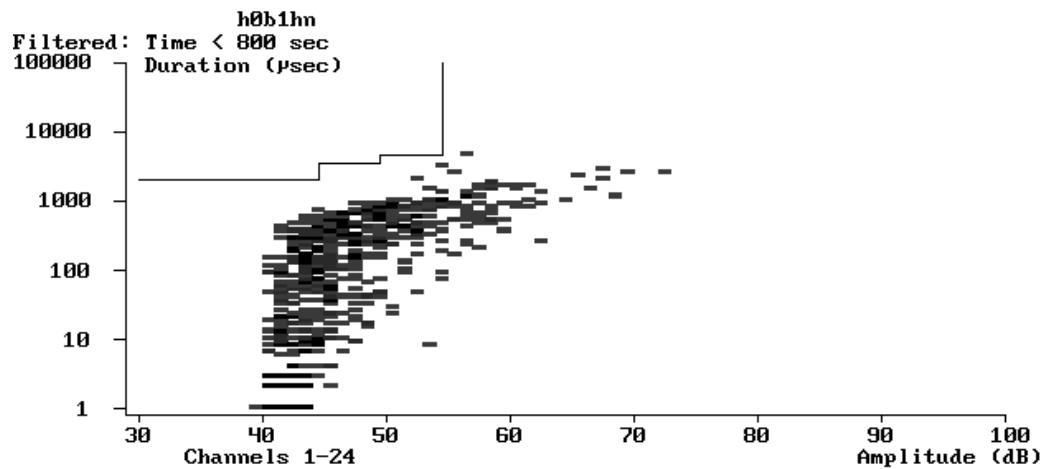


Figure 4.43 Log duration vs. amplitude plot of Test H0B1N, t=800 sec, all channels.

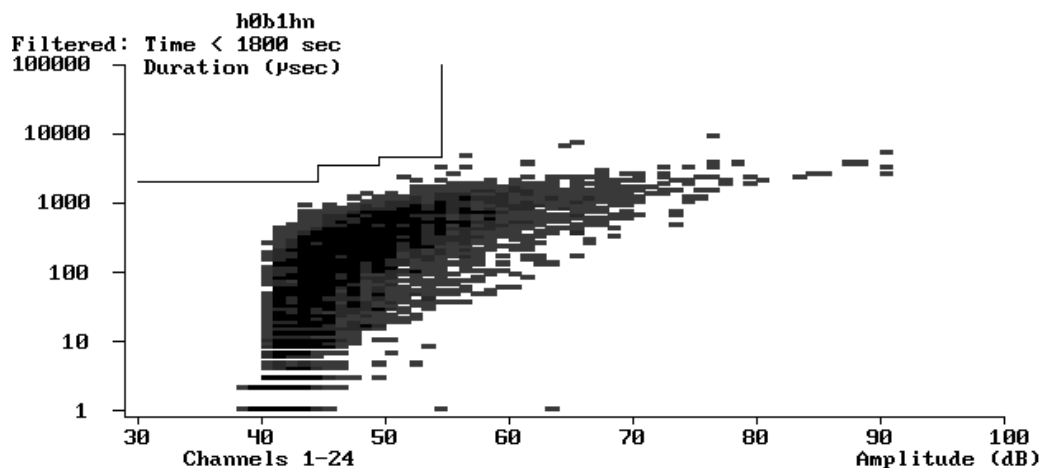


Figure 4.44 Log duration vs. amplitude plot of Test H0B1N, t=1800 sec, all channels.

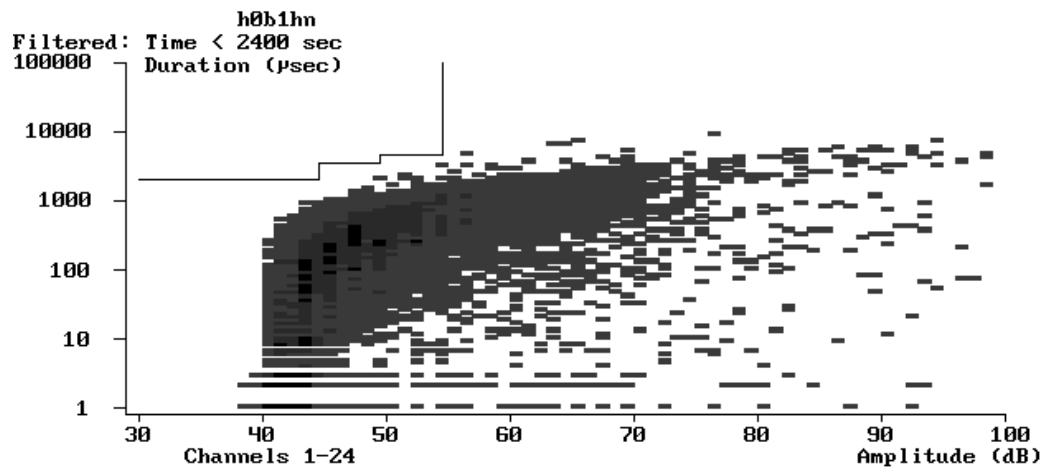


Figure 4.45 Log duration vs. amplitude plot of Test H0B1N, t=2400 sec, all channels.

4.3 SUMMARY OF PARAMETRIC TESTS

A summary of the load, cumulative signal strength, and historic index for each of the parametric tests is presented in Table 4.1. From the parameters shown in the table, the summary plots shown on Figures 4.46 through 4.48 were obtained. These figures provide an idea of the consistency of the results obtained in the parametric tests.

Table 4.1 Summary of results of parametric tests.							
TEST #	LOAD			Σ SIGNAL		HISTORIC INDEX	
		kip		STRENGTH			
	Onset of	*1st	Ult.	Onset	After 1st	Onset	1st
	AE	crack		of AE	crack	of AE	crack
M0B0S	140	221 F	339	1000	135000	4.0	21.0/48.0 [†]
M0B0N	121	211 S	383	2000	155000	3.6	19.0
M0B1N	139	202 S	460	2000	20000	2.8	2.8
M0B1S	171	211 S	474	4000	50000	4.0	6.5
H0B0N	161	222 S&F	341	3000	112000	3.8	28.0
H0B0S	144	203 S	391	4000	80000	10.0	44.0
H0B1S	141	201 S	467	500	18000	3.0	3.5
H0B1N	141	210 S	472	1000	27000	2.5	2.5

* F = flexure crack, S = shear crack.

† Test M0B0S also presents a value of historic index for the 1st shear crack.

Figure 4.46 shows the load at the onset of acoustic emission as a ratio to the first cracking load and the ultimate load. Tests in which shear cracks occurred first are shown with a different marker than the tests in which flexure cracks were first visible at the surface.

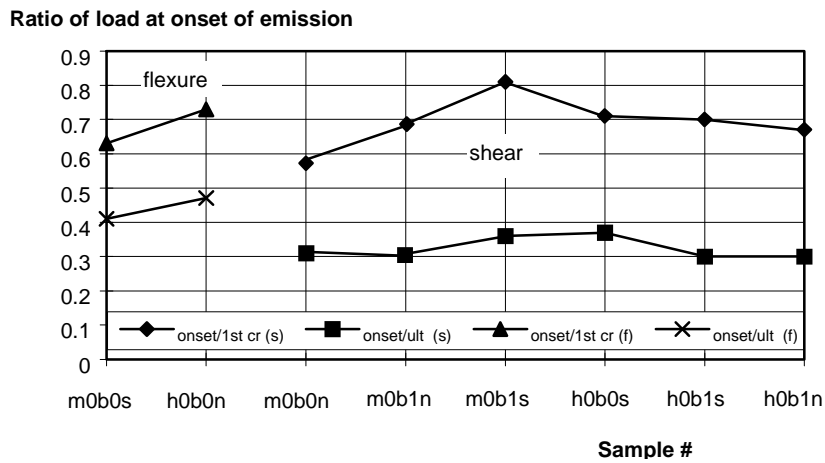


Figure 4.46 Ratio of load at onset of emission to first cracking load and to ultimate load as a function of test sample.

Figure 4.47 shows the average cumulative signal strength value of the most active channel for each test on a logarithmic scale, immediately after onset of emission and after first cracking.

A plot of the historic index value after onset of AE and after first cracking for each test, is presented in Figure 4.48.

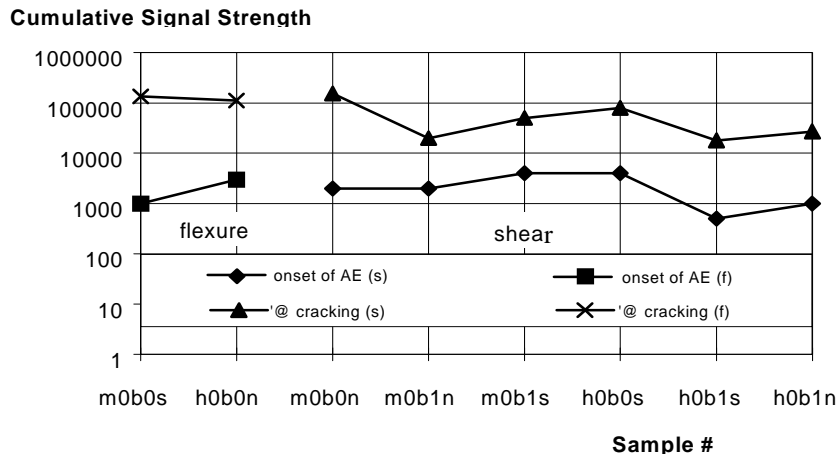


Figure 4.47 Cumulative signal strength at onset of AE and at first cracking as a function of test sample.

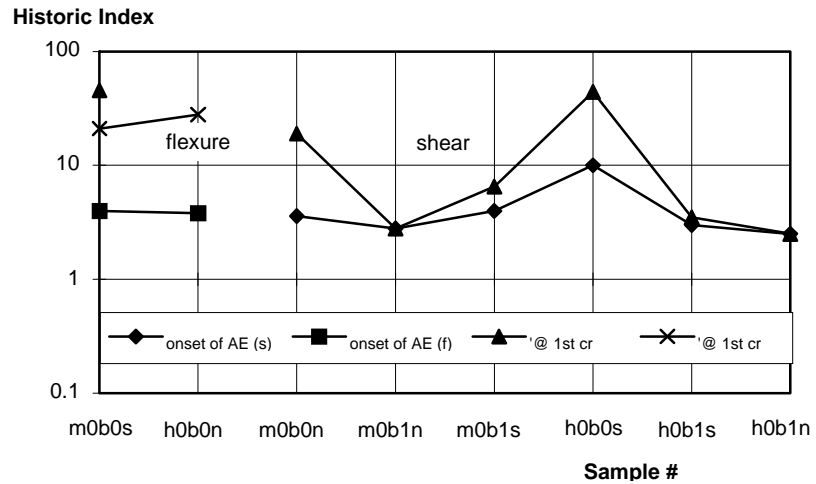


Figure 4.48 Historic index at onset of AE and at first cracking as a function of test sample.

4.4 GROUP II TESTS - SOURCE LOCATION AND MOMENT TENSOR ANALYSIS

The purpose of this group of tests is to compare the results of a moment tensor analysis with actual crack types and patterns visible at the surface of the beam. The results presented in this section were performed using the digital MISTRAS 6 channel System on two tests: L4B0S and L4B1N. The monitoring was concentrated in the maximum moment region where known cracks of flexure type were expected.

The waveforms were recorded in their entirety and post-analyzed for amplitude and time selection. Then, the selected values were processed by the Sigma program from Physical Acoustics Corporation in order to obtain information on source location and type of crack. The events were located in space and classified as flexure, mixed or shear mode according to the percent value of the first eigenvalue decomposition. For comparison, the actual crack pattern is shown on the location plot for each test.

4.4.1 Test L4B0S

Six sensors are required for this type of test. Three were attached to each side of the web in the flexure zone. The arrangement of the sensors is shown schematically on Figure 3.5. In this test, the first crack occurred at a load of 123 k. The ultimate load resisted by the beam was 198 k.

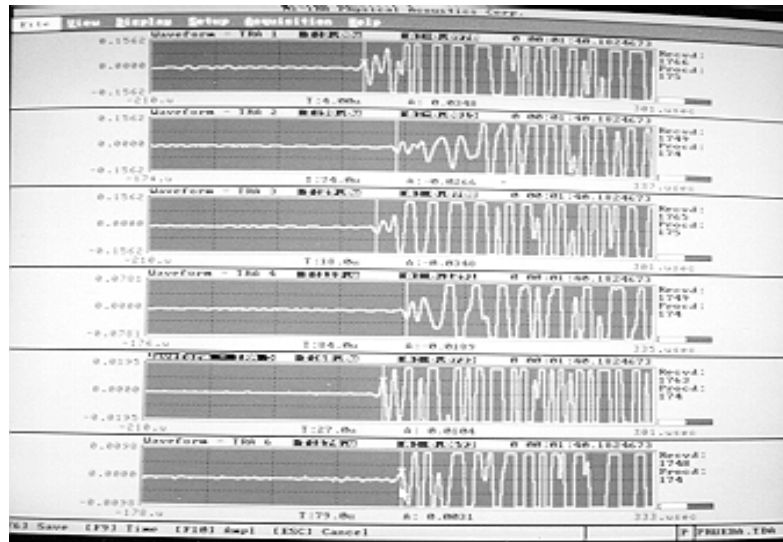


Figure 4.49 Typical waveforms used for source location and moment tensor analysis.

Typical waveforms from an event, obtained using the program MT-TRA for six channels, are shown in Figure 4.49. The vertical axis for each channel has to be scaled manually to account for differences in sensor sensitivity.

The signals were processed using a threshold of detection of 0.05 volts (54 dB), which narrows the selection of events to a few dozens rather than the several thousands typical of a test. This relatively high threshold was selected to facilitate the analysis, since these tests were run as a demonstration of the capabilities of the Moment Tensor Analysis software, rather than to obtain exact results. At the time of the tests, the software was being improved to automate the analysis of the selected events. This would make the task of obtaining precise location of all possible events, fairly trivial.

Once the signals were processed, the P-wave amplitudes and times of arrival were recorded. The Sigma program was run for every event selected, and an output like the one shown on Illustration 4.1 was obtained for every valid event. The output shows the sensor coordinates (transducer position), and orientation or direction cosine (transducer face direction). From this output, source location coordinates and type of crack were extracted.

```

*** AE Source Inversion SiGMA Solution List ***
( Date, 04-04-1997 Time, 18:48:45 )
[ Channel Data List ]
ch.| Transducers Position | Transducers Direction | Arrival Time | Amplitude
   | x   y   z   | x   y   z   | (sec) | (volts)
11 | 0.914 0.203 0.000 | 0.0000 0.0000 1.0000 | 0.430000E-04 | -0.0336
12 | 0.914 0.000 0.000 | 0.0000 0.0000 1.0000 | 0.000000E+00 | 0.0183
13 | 0.000 0.013 0.000 | 0.0000 0.0000 1.0000 | 0.121000E-03 | 0.0186
14 | 0.000 0.203 0.152 | 0.0000 0.0000 -1.0000 | 0.130000E-03 | -0.0098
15 | 0.000 0.000 0.152 | 0.0000 0.0000 -1.0000 | 0.111000E-03 | -0.0089
16 | 0.914 0.203 0.152 | 0.0000 0.0000 -1.0000 | 0.510000E-04 | -0.0113

* Velocity of P-wave : 4000.0 (m/sec)
* Poisson's Ratio : 0.20000

[ Step 1 : AE Source Location ---> Completed ]
Source ( x , y , z ) = ( 0.720 , -0.238 , 0.041 )

[ Step 2 : Moment Tensor Solution ---> Completed ]
***** MOMENT TENSOR *****
-0.0140 -0.0170 0.0393
          -0.0103 -0.0892
sym.                1.0000
*****

[ Step 3 : Eigen Value Analysis ---> Completed ]
Eigen Value | max | mid | min
Eigen Vector x | 0.0397 | 0.7386 | 0.6730
Eigen Vector y | -0.0877 | -0.6684 | 0.7387
Eigen Vector z | 0.9954 | -0.0884 | 0.0383

< Composition Ratios of Eigen Value >
Shear : 2.68 % | CLVD : 65.11 % | Mean : 32.22 %

```

Illustration 4.1 Sample output of program Sigma.

In the last row of the output shown in Illustration 4.1 is the % shear value. A low % shear value (between 0 and 40%) means the event is of flexure type, while a high % shear value (between 60 and 100%) means the event is a shear type. Between 40 and 60% it is considered of mixed mode. Table 4.2 shows the list of the coordinates and event type for each of the 24 valid events of the test.

Table 4.2 Event coordinates and type, Test L4B0S.

EVENT	X COOR	Y COOR	Z COOR	TYPE
1	0.72	-0.238	0.041	F
2	-0.102	-0.859	-0.005	Mixed
3	-1.912	-4.136	-1.342	F
4	0.472	-0.09	0.044	F
5	0.568	-0.192	0.079	F
6	0.561	-0.142	0.041	F
7	0.732	-0.296	0.029	F
8	0.822	-0.122	0.03	F
9	0.832	-0.16	0.068	F
10	0.435	-0.204	0.079	Mixed
11	0.331	-0.749	-0.099	F
12	0.415	-0.271	-0.061	Mixed
13	0.443	-0.292	0.096	F
14	0.42	-0.233	0.088	F
15	0.278	-0.567	-0.072	F
16	0.412	-0.209	0.056	F
17	-0.697	-1.27	0.282	F
18	0.049	-0.017	0.116	F
19	0.419	-0.173	0.055	F
20	0.369	-0.118	-0.104	F
21	0.651	-0.175	0.039	F
22	0.71	-0.143	0.075	F
23	0.357	-0.176	-0.192	F
24	0.638	-0.09	0.048	F

Figure 4.50 shows the east face view of the beam with the crack pattern superimposed onto the plotted located sources. Cracks from both faces, east and west, are marked, being differentiated by the weight of the line. The bottom of the beam is shown with a heavy line at a distance of -0.3 m relative to the [0,0,0] coordinate.

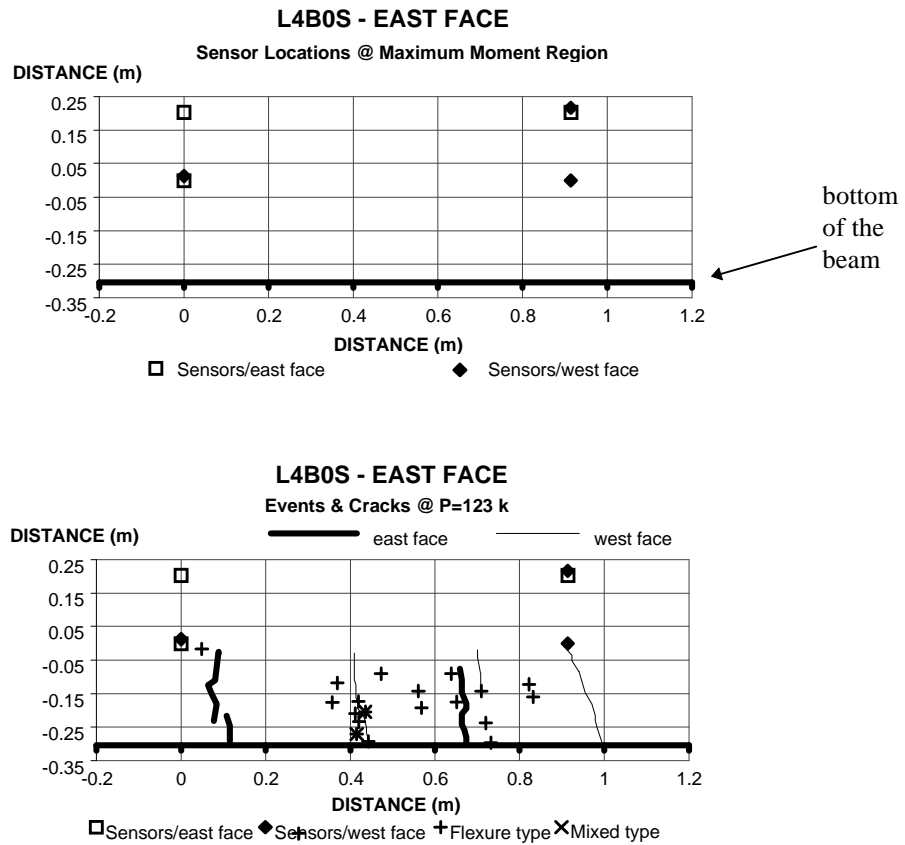


Figure 4.50 Location of events and crack pattern of Test L4B0S.

The sensors are represented by the hollow square and solid rhomboid, and they define the maximum moment region. The events plotted are cumulative from the beginning of the test up to the 123 k load interval when first cracks appeared on the surface as marked on the figure.

It can be noted that the events located on Figure 4.50 correlate very well with the crack pattern superimposed on the plot. However, they are concentrated in the middle region between the sensors. Very few events were located near the extreme cracks. This could be explained by attenuation of the signals traveling from one extreme to the other. If a crack is developing in the extreme of the monitored area, the signal will be strong in the sensors near that extreme, but it will attenuate during its travel to the sensors in the other extreme. Greater sensitivity of the method, then, can be expected in a region around the center of gravity of the location of the sensors.

4.4.2 Test L4B1N

Test L4B1N required six sensors as in the previous test. The location of the sensors is shown schematically in Figure 3.6. For this test, three faces were covered: either side of the web and the bottom face. The first shear cracks occurred at a load of 130 k but the beam was monitored for one more load interval up to a load of 135 k. The crack pattern was followed to the load of 160 k. The maximum load resisted by the beam was 226 k. Table 4.3 shows the results for the location and crack classification for the test with the corresponding load interval.

Following from the discussion of the previous test, greater sensitivity is expected for Test L4B1N. Two sensors are now covering the bottom face, bringing the center of gravity of the location of the sensors closer to the bottom of the beam, where most of the acoustic emission will occur.

The same criteria as described in Section 4.4.1, was applied for the selection of the events, using the same threshold in the MT-TRA program. The increased number of events obtained in this test, compared to Test L4B0S, is explained by the greater sensitivity due to the arrangement of the sensors as discussed in the previous paragraph.

Table 4.3a Event coordinates and type, Test L4B1N (continued on next page as Table 4.3b).

EVENT	X COOR	Y COOR	Z COOR	TYPE	Load Interval
1	0.775	0.107	0.032	F	
2	-1.61	-1.176	1.549	F	
3	0.499	0.103	0.276	F	
4	0.317	0.063	0.133	Mixed	
5	0.699	0.136	-0.001	Mixed	70 k
6	0.868	0.096	0.059	F	
7	0.383	0.269	0.015	F	
8	0.652	-0.02	0.265	S	
9	0.52	0.192	0.032	Mixed	
10	0.26	0.189	0.021	F	
11	-0.204	-0.525	0.577	F	
12	0.379	0.081	0.2	F	
13	0.599	0.217	-0.034	F	90 k
14	0.07	-0.031	0.189	F	
15	0.404	0.072	0.124	F	
16	0.452	0.185	0.103	Mixed	
17	0.171	-0.011	0.089	F	
18	-18600	-3200	-3300	F	
19	0.374	0.271	0.08	S	
20	0.384	0.133	0.083	Mixed	
21	0.749	0.079	0.113	S	
22	0.116	-0.551	-0.022	F	
23	-2.413	0.497	-1.491	F	
24	0.488	0.138	0.556	F	110 k

Table 4.3b Event coordinates and type, Test L4B1N (continued).

EVENT	X COOR	Y COOR	Z COOR	TYPE	Load Interval
					110 k
25	0.392	0.174	0.093	Mixed	
26	0.487	0.133	0.193	Mixed	
27	0.671	0.15	0.05	F	
28	0.298	0.01	0.08	F	
29	0.217	0.119	0.134	S	
30	0.532	0.098	0.222	Mixed	
31	0.009	0.129	-0.008	S	
32	0.439	0.191	0.063	S	120 k
33	0.45	-0.1	0.83	F	
34	0.385	0.004	0.255	Mixed	
35	0.443	0.036	0.227	Mixed	
36	0.408	-0.421	0.111	F	
37	-1.948	-1.345	-1.666	F	
38	0.61	0.123	0.233	Mixed	
39	0.39	0.141	0.043	F	
40	0.407	-0.023	0.106	F	
41	0.397	0.051	0.053	F	
42	0.375	0.083	0.074	F	
43	0.574	0.114	0.035	F	
44	0.373	0.11	0.243	F	
45	0.197	0.139	0.102	S	
46	0.2	0.045	0.111	F	
47	0.237	0.098	0.092	F	
48	0.759	0.287	-0.033	S	
49	0.391	0.168	0.03	F	
50	0.149	0.165	-0.02	F	
51	0.41	0.059	0.1	F	
52	0.23	0.054	0.071	F	
53	0.453	0.282	0.09	S	
54	0.279	0.316	0.019	F	130 k
55	0.42	-0.072	0.495	F	
56	0.38	0.039	0.155	F	
57	0.231	0.01	0.108	F	
58	0.416	0.034	0.08	F	
59	0.4	-0.014	0.243	F	
60	0.41	0.066	0.083	F	
61	0.233	0.06	0.113	F	
62	0.214	0.15	0.055	F	
63	0.39	0.092	0.038	F	
64	0.225	0.096	0.061	F	
65	0.211	0.014	0.27	Mixed	
66	0.23	-0.007	0.235	Mixed	
67	0.376	0.048	0.087	F	
68	0.22	0.075	0.091	F	
69	0.191	0.014	0.094	F	
70	0.202	0.029	0.093	F	
71	0.616	0.089	0.009	F	
72	0.387	0.049	0.037	F	
73	0.229	0.008	0.189	Mixed	135 k

←
first
crack

In order to obtain groups of events corresponding to a specific load interval, the test was subdivided. Sub-tests were run, starting a new test for every interval marked on the table. The events were not recorded with a specific load value. Instead, they were recorded during the load intervals shown. In this way, a representation of the events popping up in what will be the surface cracks, could be made.

The events listed in Table 4.3 are plotted in Figures 4.52, 4.56 and 4.60. Figure 4.51 shows the location of the sensors viewing from the west face. The sensors located on the east face are shown with a different marker. The bottom of the beam is represented in the graph by a heavy line.

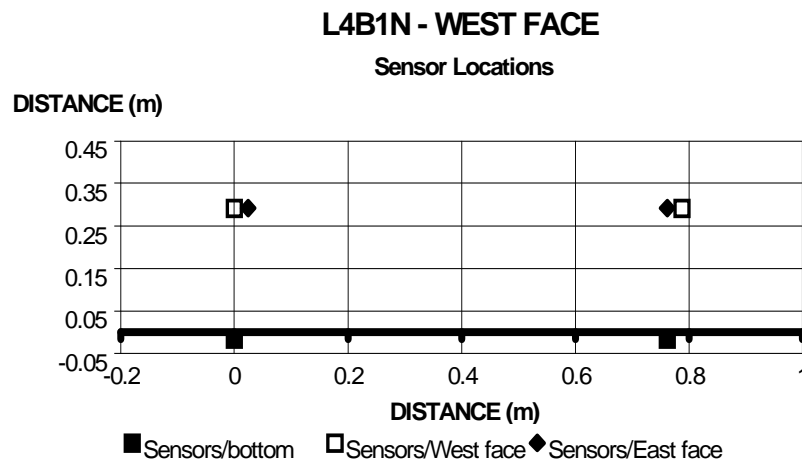


Figure 4.51 Sensor locations of Test L4B1N.

In Figure 4.52, the plotted events are cumulative up to a load of 110 k. At this loading there was no visible crack. A few events are of shear and mixed type. These events may correspond to friction between the concrete and the bonded strands, during elongation under flexure.

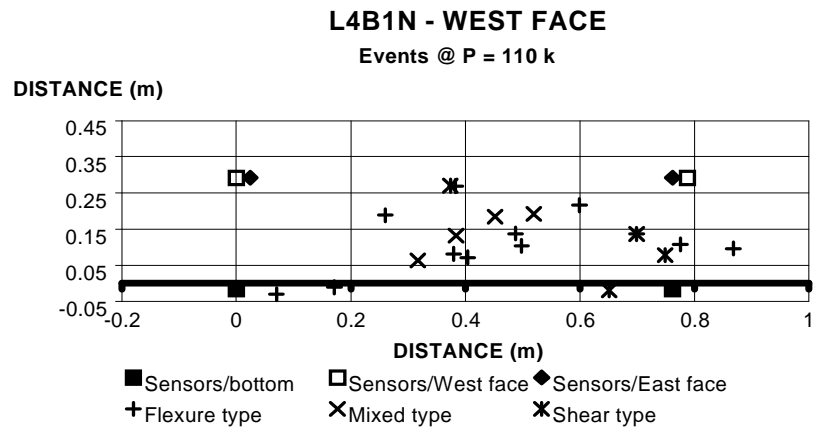


Figure 4.52 Event locations at P=110 k, Test L4B1N.

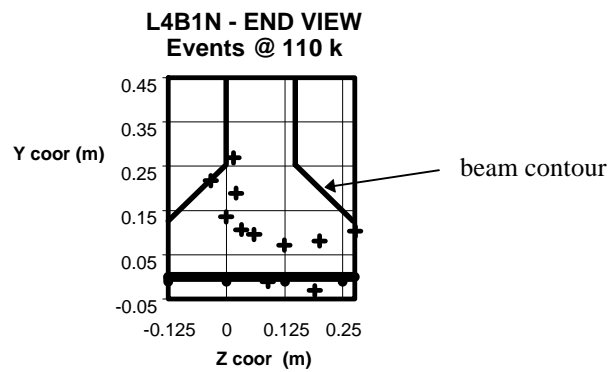


Figure 4.53 Event locations at P=110 k, Test L4B1N, end view.

Figures 4.54 and 4.55 show the first cracks marked on the surface of the beam, on the west and east faces respectively.

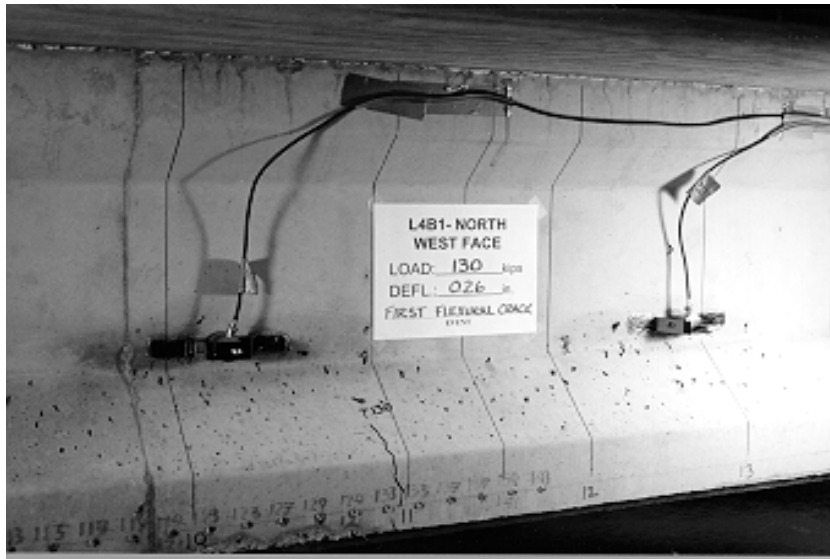


Figure 4.54 West face view of the first crack at P=130 k, Test L4B1N.

Figure 4.56 shows the plot of the located events along with the superimposed crack pattern at the first cracking load. The events are cumulative up to the load P=130 k. The alignment of the events follows very closely the crack pattern marked on the surface. Figure 4.57 is the complementary end view to Figure 4.56. It is useful for comparison of the crack growth, as it shows how the events are filling the area, forming the crack plane.

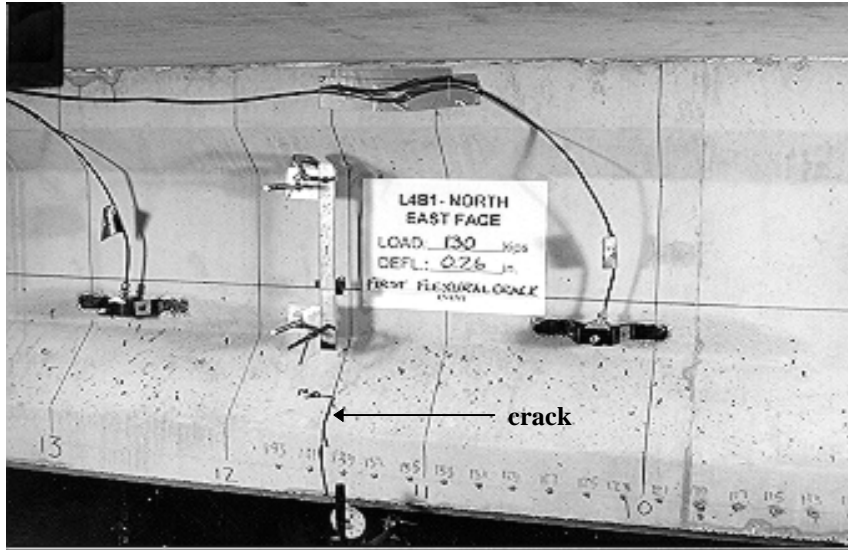


Figure 4.55 East face view of the first crack at P=130 k, Test L4B1N.

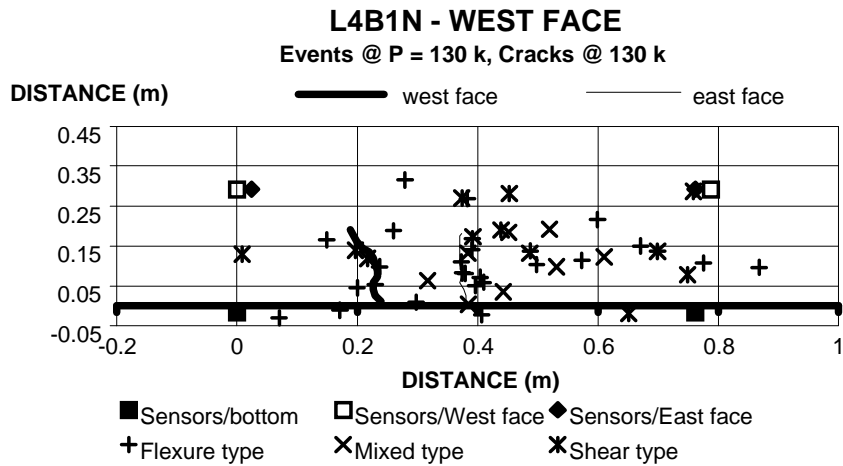


Figure 4.56 Event locations and crack pattern at P=130 k, Test L4B1N.

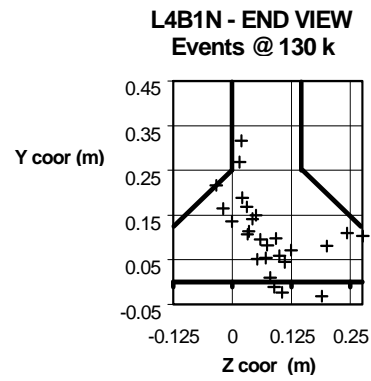


Figure 4.57 Event locations at $P=130$ k, Test L4B1N, end view.

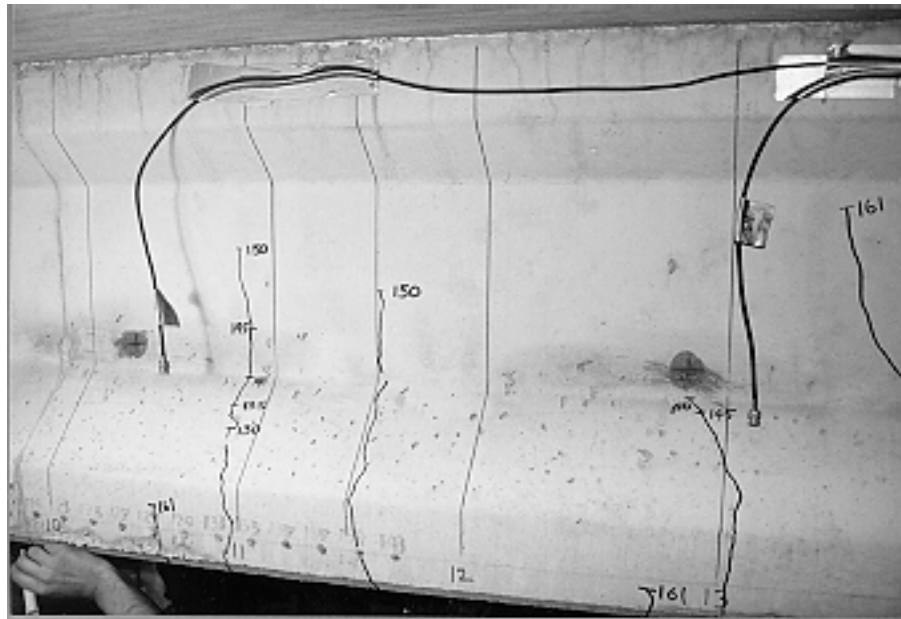


Figure 4.58 West face view of cracks at $P=161$ k, Test L4B1N.

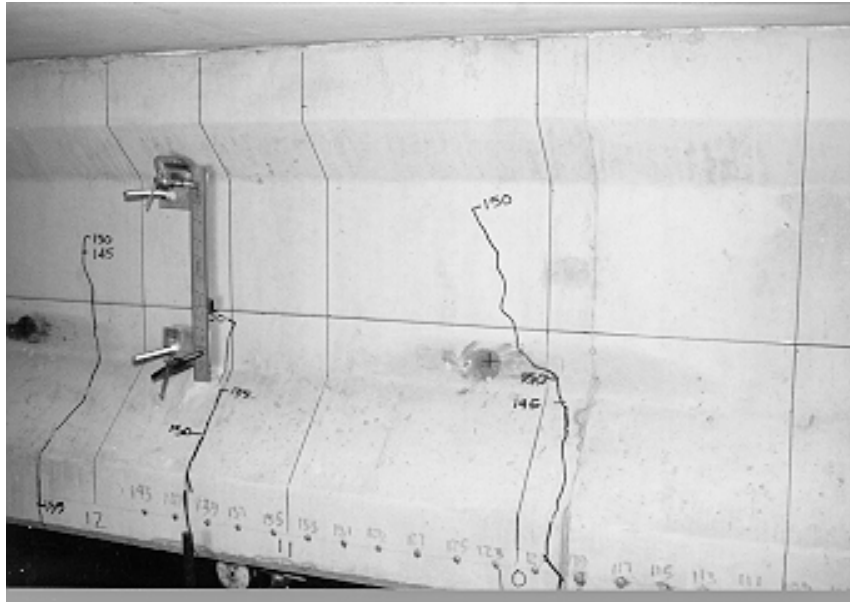


Figure 4.59 East face view of cracks at $P=161$ k, Test L4B1N.

The tests were monitored after the first cracking load up to the next loading interval of 135 k. The crack pattern, however, was followed until a load of 161 k. Figures 4.58 and 4.59 present the marked cracks on the beam from both faces.

Figure 4.60 shows the located events up to a load of 135 k and the cracking pattern of the beam at a load of 160 k. A good agreement is seen between the located events and the actual crack pattern from the beam.

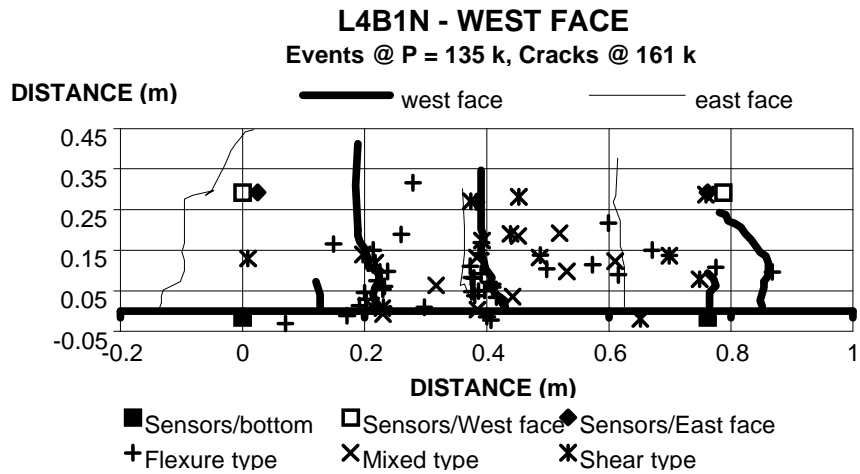


Figure 4.60 Event locations at P=135 k and crack pattern at P=160 k, Test L4B1N.

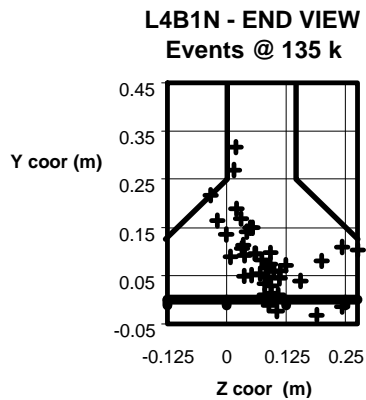


Figure 4.61 Event locations at P=161 k, Test L4B1N, end view.

The side view corresponding to the location of the events at the load $P=161$ k is shown on Figure 4.61. It is clearly seen that the crack planes shown by the marks correspond to the events within the bottom flange of the section.

A close agreement between the located events and the crack pattern is noted from the elevation view (west face) of cracking, shown in Figure 4.60. Some cracks are followed very closely by the marks on the plot. Since the cracks are seen in both faces of the beam, it can be expected to obtain events located throughout the area of the beam. This can be observed comparing Figures 4.53, 4.57 and 4.61.

CHAPTER 5

CONCLUSIONS AND RECOMMENDATIONS

5.1 CONCLUSIONS

In the parametric tests, the cumulative signal strength vs. time plots show clear warning signs prior to the appearance of the cracks at the surface. This effect is marked by an increase in the slope of the curve at the point called the “onset of acoustic emission”. It is believed that this corresponds to the formation of the characteristic microcrack network. After this point, the emission grows in a regular manner until the visible cracks are formed. Development of visible cracks corresponds to a sudden large increase in the cumulative signal strength. The historic index vs. time graphs show the same information in a different way. The onset of acoustic emission, and the initiation of cracking occur as peak values, usually greater than 3 and 10 respectively.

The log duration vs. amplitude relationships are presented for all parametric tests. They show how characteristic hits are triggered after the onset of emission. The high data rates which occur after onset of emission result in overlapping and truncated hits accompanied by an increasing number of high amplitude hits. The high data rates are explained by the rapidly forming network of microcracks and associated wave reflection. The difference is clearly marked after visible cracking, when the scatter of data is accentuated by the enormous

release of energy during microcrack interconnection and subsequent crack growth.

During the test program, the sensor located at the end of the beam did not detect any particular events related to slippage of the prestressing tendons. This was corroborated by the null measurements of relative displacement between the tendons and concrete recorded by the instrumentation directly attached to the free end of the beams.

In the two tests directed towards source location and Moment Tensor Analysis, the results show a good agreement with the crack pattern visible at the surface of the beam. This is indicated in the figures showing events superimposed with the marked cracks. The great percentage of events were marked as flexure type, as would be expected from the loading arrangement. In test L4B1N a few events were classified as mixed type and some even as shear type. These events are located in a scattered manner and may well be due to errors in the selection of the events or shear friction between the strands and the concrete due to elongation of the prestressing strands in the flexure zone.

From the test program reported in this thesis, the following conclusions can be drawn:

1. Cracks in prestressed concrete elements can be predicted by acoustic emission. The onset of acoustic emission indicates initiation of a network of microcracks in the concrete. Cumulative signal strength, large amplitude hits, and historic index can be used to detect crack development.

2. Reliable acoustic emission signals are detected in concrete under compression. Prestressed concrete, due to the precompression exerted by the prestressing strands, promotes hit detection and wave travel along considerable lengths of the element.
3. Scatter in the log duration vs. amplitude graphs is an indication of high data rates, caused by crack development. Microcracking is indicated by overlapping and truncated hits. Crack formation is accompanied by overlapping hits and a large number of truncated hits, including some of high amplitude.
4. The moment tensor analysis technique predicts the position and growth of a crack, together with type classification.
5. Identification of the presence, type and location of a crack, prior to its appearance at the surface, will be of benefit in field testing. Early warning of cracking and information concerning location of the cracks, will permit more efficiency in handling remedial action or scheduled repairs.

5.2 RECOMMENDATIONS

The following recommendations are offered to future researchers undertaking experimental work in the area of acoustic emission in prestressed concrete. These are based on the experience gained during the testing program, and analysis of the obtained data.

- The equipment used for the tests must have adequate capacity to handle large quantities of information at high data rates. This means that large disk storage capacity and a fast processor are essential. This is a more important issue with prestressed concrete in contrast with other materials such as steel or reinforced plastics.

- Higher thresholds can be used to reduce the severity of the above mentioned problem. It was demonstrated that good signal reception was achieved during these tests. Thresholds as high as 45 or 50 dB can be used for noisy situations, such as in field testing or when only rough indications of activity are desired. For detailed monitoring, the 40 dB threshold level used for these tests, proved to be a good value.

- A shorter hit definition time should be considered, compared to the value of 400 μ s used for these tests. A shorter time might reduce the number of overlapping hits.

- Instrumentation with a shorter rearm time should be used. The parametric tests used an instrument with a 200 μ s rearm time. A shorter rearm time will reduce the number of truncated hits.

- All the equipment must be kept in calibration. It is important to arrange sensors with the same sensitivity in specific areas. For example, when doing a moment tensor analysis test, all sensors of a given array should have the same sensitivity.

- Attachment of the sensors to the surface must be done carefully in order to avoid bad or damaged areas on the element. The surface must be thoroughly cleaned and loose particles removed prior to attaching the sensors.

- Ambient noise must be determined and, during the test, all significant changes must be noted in the test log for later interpretation.

- Finally, it is recommended that the researcher subdivide the test data in sub-files and later assemble them as required, rather than to work with one long file containing the complete test.

REFERENCES

1. Halmshaw, R., “*Non-Destructive Testing*”, 2nd ed. **Edward Arnold**, Great Britain, 1987.
2. ASME, Sc. V art. 11 and art. 12. **American Society of Mechanical Engineers**, New York, NY.
3. SPI, “*Recommended Practice for Acoustic Emission Testing of Fiberglass Reinforced Plastic Resin (RP) Tanks/Vessels*”. **The Society of the Plastics Industry**, Reinforced Plastics/Composites Institute, New York, NY, 1987.
4. Mindess, S., “*Concrete*”. **Prentice-Hall Inc.**, Englewood Cliffs, NJ, 1981.
5. Fowler, T., Blessing, J., and Conslik, P., “*New Directions in testing*”. **Third International Symposium on Acoustic Emission from Composite Materials**, AECM-3, Paris, France, July 17-21, 1989.
6. AAR, “*Procedure for Acoustic Emission Evaluation of Tank Cars and IM101 Tanks, Issue 5*”. **Association of American Railroads**, Mechanical Division, Washington, DC, January 1996.
7. ASTM, “*Standard Practice for Acoustic Emission Examination of Fiberglass Reinforced Plastic Resin (FRP) Tanks/Vessels, E 1067*”. **American Society for Testing and Materials**, Philadelphia, PA.
8. ASME, “*Acceptance Test Procedure for Class II Vessels, Article RT-6, Section X, Boiler and Pressure Vessel Code*”, **American Society of Mechanical Engineers**, New York, NY.
9. Uomoto, T., Sato, S., and Yamamoto, S., “*Determination of Applied Compressive Stress in Concrete Structures by Acoustic Emission Measurements*”. **Progress in Acoustic Emission III**, The Japanese Society of NDI, p. 538, 1986.

10. Chen, H., Cheng, C., and Chen, S., “*Determination of Fracture Parameters of Mortar and Concrete Beams by Using Acoustic Emission*”. **Materials Evaluation**, The American Society for Nondestructive Testing, p 888, July 1992.
11. Shigeishi, M., Ohtsu, M., and Yuyama, S., “*Sigma Analysis of Fracture Process Zone in Notched Concrete Beams*”. **Fifth International Symposium on Acoustic Emission From Composite Materials**, The American Society for Nondestructive Testing, p.403, Sundsvall, Sweden, July 1995.
12. Nesvijski, E., “*On the Application of the Acoustic Emission Method for the Prognosis of Hard Concrete at Early Ages*”. **Fifth International Symposium on Acoustic Emission From Composite Materials**, The American Society for Nondestructive Testing, p.385, Sundsvall, Sweden, July 1995.
13. Ohtsu, M., Murakami, Y., and Yuyama, S., “*AE Generating Behavior Under Concrete Placement and Application to Process Control*”. **Fifth International Symposium on Acoustic Emission From Composite Materials**, The American Society for Nondestructive Testing, p.385, Sundsvall, Sweden, July 1995.
14. Nielsen, J., and Griffin, D., “*Acoustic Emission of Plain Concrete*”. **Journal of Testing and Evaluation**, JTEVA, Vol. 5, No. 6, Nov. 1977, pp. 476-483.
15. Baron, R., and Worthington, W., “*Corrosion Detection in Concrete Water Pipes*”. **Underground Construction**, February 1997.
16. Hick, H., Willer, H., Winter, E., and Simacek, F., “*Acoustic Emission Measurements on Bridges*”. **Journal of Acoustic Emission**, Vol. 10, No.3/4.
17. Pérami, R., and Bosc, F., “*Effects of Silica Fume Additions on Mechanical Performances of Concrete Composites. Investigations by AE and gas permeability*”. **Fifth International Symposium on Acoustic Emission From Composite Materials**, The American Society for Nondestructive Testing, p.322, Sundsvall, Sweden, July 1995.

18. Rudzinski, L., and Golaski, L., "*Synthetic Fiber Reinforced Cement Composites - A Study of Fracture Processes by the AE Method*". **Fifth International Symposium on Acoustic Emission From Composite Materials**, The American Society for Nondestructive Testing, p.341, Sundsvall, Sweden, July 1995.
19. Matsuyama, K., Ishibashi, A., and Ohtsu, M., "*Rate Process Analysis of AE Activity in Core Test of Deteriorated Concrete*". **Progress in Acoustic Emission VI**, The Japanese Society of NDI, p. 479, 1992.
20. Redjel, B., "*Use of Acoustic Emission to Study Fatigue Damage of Concrete*". **Fifth International Symposium on Acoustic Emission From Composite Materials**, The American Society for Nondestructive Testing, p. 312, Sundsvall, Sweden, July 1995.
21. Niseki, S., Satake, M., and Gohke, M., "*Quick Detection of Alkali-Aggregate Reaction by AE Monitoring*". **Progress in Acoustic Emission V**, The Japanese Society of NDI, p. 331, 1990.
22. Jeong, H., Takashaki, H., and Teramura, S., "*Low Temperature Fracture Behavior and AE Characteristics of Autoclaved Aerated Concrete (AAC)*". **Progress in Acoustic Emission III**, The Japanese Society of NDI, p. 529, 1986.
23. Uomoto, T., and Kato, H., "*Drying Shrinkage of Concrete and Acoustic Emission*". **Progress in Acoustic Emission V**, The Japanese Society of NDI, p. 325, 1990.
24. Hawkins, N., McCabe, W. and Nobuta, Y., "*Use of Acoustic Emission to Detect Debonding of Reinforcing Bars in Concrete*". **Progress in Acoustic Emission IV**, The Japanese Society of NDI, p. 342, 1988.
25. Murakami, Y., Yamashita, H., and Ohtsu, M., "*AE Properties of Concrete with Corroded Reinforcement*". **Progress in Acoustic Emission VI**, The Japanese Society of NDI, p. 471, 1992.
26. Uomoto, T., and Kawakami, T., "*Behavior of Concrete Specimens in Splitting Tensile Test*". **Progress in Acoustic Emission IV**, The Japanese Society of NDI, p. 336, 1988.

27. Fowler, T., Blessing, J., Conslik, P., and Swanson, T., "*The MONPAC System*". **Journal of Acoustic Emission**, Vol. 8, No. 3
28. Ohtsu, M., "*Source Inversion Procedure for Acoustic Emission*". **Progress in Acoustic Emission IV**, The Japanese Society of NDI, p. 67, 1988.